Journal of Medicinal Chemistry

Article

Development of a high affinity PET radioligand for imaging cannabinoid subtype 2 receptor (CB)

Rares-Petru Moldovan, Rodrigo Teodoro, Yongjun Gao, Winnie Deuther-Conrad, Mathias Kranz, Yuchuan Wang, Hiroto Kuwabara, Masayoshi Nakano, Heather Valentine, Steffen Fischer, Martin G Pomper, Dean F Wong, Robert F. Dannals, Peter Brust, and Andrew G. Horti

J. Med. Chem., **Just Accepted Manuscript** • DOI: 10.1021/acs.jmedchem.6b00554 • Publication Date (Web): 08 Aug 2016

Just Accepted

ACS Publications

Journal of Medicinal Chemistry is published by the American Chemical Society. 1155 Sixteenth Street N.W., Washington, DC 20036

Development of a high affinity PET radioligand for imaging cannabinoid subtype 2 receptor (CB_2)

Rareş-Petru Moldovan[1,], Rodrigo Teodoro[1], Yongjun Gao[2], Winnie Deuther-Conrad[1], Mathias Kranz[1], Yuchuan Wang[2], Hiroto Kuwabara[2], Masayoshi Nakano[2], Heather Valentine[2], Steffen Fischer[1], Martin G. Pomper[2], Dean F. Wong[2], Robert F. Dannals[2], Peter Brust[1], Andrew G. Horti[2,]**

[1] Helmholtz-Zentrum Dresden-Rossendorf e. V., Institute of Radiopharmaceutical Cancer Research, Leipzig, Germany

[2] Johns Hopkins School of Medicine, Department of Radiology, Baltimore, USA

ABSTRACT: Cannabinoid receptors type 2 (CB_2) represent a target with increasing importance for neuroimaging due to its upregulation under various pathological conditions. Encouraged by preliminary results obtained with [^{11}C](*Z*)-*N*-(3-(2-methoxyethyl)-4,5-dimethylthiazol-2(3*H*)-ylidene)-2,2,3,3-tetramethyl-cyclopropanecarboxamide ([^{11}C]A-836339, [^{11}C]**1**) in a mouse model of acute neuroinflammation (induced by lipopolysaccharide, LPS), we designed a library of fluorinated analogs aiming for an [^{18}F]-labeled radiotracer with improved CB_2 binding affinity and selectivity. Compound (*Z*)-*N*-(3-(4-fluorobutyl)-4,5-dimethylthiazol-2(3*H*)-ylidene)-2,2,3,3-tetramethyl-cyclopropanecarboxamide (**29**) was selected as a ligand with the highest CB_2 affinity (K_i = 0.39 nM) and selectivity over CB_1 (factor 1000). [^{18}F]**29** was prepared starting from the

bromo precursor (**53**). Specific binding was shown *in vitro* whereas fast metabolism was observed *in vivo* in CD-1 mice. Animal PET revealed a brain uptake comparable to [^{11}C]**1**. In the LPS treated mice, a 20-30% higher uptake in brain was found in comparison to non-treated mice (n = 3, $P<0.05$).

INTRODUCTION

Since its isolation and elucidation of the structure in 1964 by Mechoulam and co-workers,[1, 2] (–)-*trans*-Δ^9-tetrahydrocannabinol (THC) has been the subject of many scientific investigations due to its intriguing biological properties.[3] This led to the discovery of the endogenous cannabinoid system, which comprises a class of transmembrane proteins that belongs to the superfamily of G-protein-coupled receptors and their modulatory lipids.[4, 5] Etymologically, cannabinoid receptors are proteins that are activated by THC, the principal psychoactive constituent of the cannabis plant.[6]

Two types of cannabinoid receptors have been cloned so far, cannabinoid receptor type 1 (CB_1)[7] and cannabinoid receptor type 2 (CB_2).[8] There is evidence for further cannabinoid receptors with unclear molecular identity, collectively known as non-CB_1/CB_2 receptors.[9] The most prominent candidates are GPR55[10] and GPR119.[11] CB_1 receptors are mainly located at the terminals of central and peripheral neurons, and are the most abundantly expressed G-protein-coupled receptors in the brain.[5] Their activation is responsible for the psychotropic effect of THC.[5, 12] On the other hand, the CB_2 receptor has been categorized as the peripheral cannabinoid receptor due to its presence on the cells and tissues of the immune, reproductive, cardiovascular, gastrointestinal and respiratory systems.[12]

Although numerous reports were unable to detect CB_2 receptor in normal healthy brain, recent evidence suggests that CB_2 receptors are present in the brain under normal and in particular under pathological conditions, although to a much lesser extent than the ubiquitously expressed CB_1 receptors.[13] The role and distribution of CB_1 receptors in the living human brain have already been investigated intensively.[14, 15] Much less is known about the role and distribution of the CB_2 receptors in the human brain.[13] Low levels of CB_2 receptors are found in microglial cells,[16-18] human fetal astrocytes,[19] and human cerebral microvascular endothelial cells.[20] Overexpression of the CB_2 receptor has been found on microglia associated with neuritic plaques in Alzheimer's disease.[21] Enhanced CB_2 receptor expression, primarily on activated microglia, has been demonstrated in several other neurodegenerative disorders such as multiple sclerosis,[22, 23] Down's syndrome,[24] and Huntington's disease.[25] CB_2 expression pathologies also include traumatic brain injury,[26] neuropathic pain,[27] and HIV-induced encephalitis.[28] Significant alterations of a balance in the cannabinoid system between the levels of endogenous ligands and their receptors occur during malignant transformation in various types of cancer including brain tumors, as previously reviewed.[29, 30]

CB_2-selective ligands have gained increasing importance as therapeutic drugs for the diseases mentioned above, especially for the prevention of psychoactive side effects.[30-38] Molecular imaging with positron emission tomography (PET) of disease-specific expression of CB_2 receptors in various disorders of the central nervous system like neuroinflammation, neurodegeneration and glioma offers the potential of individualized diagnosis and therapeutic monitoring.[39]

Recently a substantial effort has been put into the development of radioligands for PET imaging of CB_2 receptors (see for reviews:[31, 40, 41]). Several radiolabeled CB_2 molecules have been developed with most representative ones depicted in Figure 1.[31, 32]

The principle of CB_2 imaging under neuroinflammatory circumstances was proven by our previous work using [^{11}C]**1**.[42] Recent PET studies revealed a significant increase in the binding of [^{11}C]**1** in a mouse model of Alzheimer's disease that was consistent with increased CB_2-immunoreactivity in astrocytes and microglia.[43] Compound [^{11}C]**2** ([^{11}C]NE40) was developed by Evens and co-workers[44] and a first-in-man study in healthy subjects was reported.[45] However, PET studies with [^{11}C]**2** did not show the expected increase of binding in subjects with Alzheimer's disease as compared to healthy controls, perhaps due to the insufficient binding affinity of the radiotracer.[46] The usefulness of CB_2 PET radiotracers in models of neuroinflammation was also demonstrated in dynamic PET studies in primates using radiolabeled triazines scaffolds ([^{18}F]**3**, Figure 1).[34, 47, 48] The most recently developed PET radioligands for CB_2 receptors are [^{11}C]**4** ([^{11}C]RS-016)[49] and [^{11}C]**5** ([^{11}C]RSR-056)[50], which demonstrated moderate specific binding in the mouse LPS mouse model of neuroinflammation.

Altogether, the importance of targeting CB_2 receptors has been shown by several groups worldwide and has been characterized in several pathological conditions in animals. However, the development of a radioligand suitable for the non-invasive investigation of the CB_2 receptor in healthy and diseased brain remains challenging.

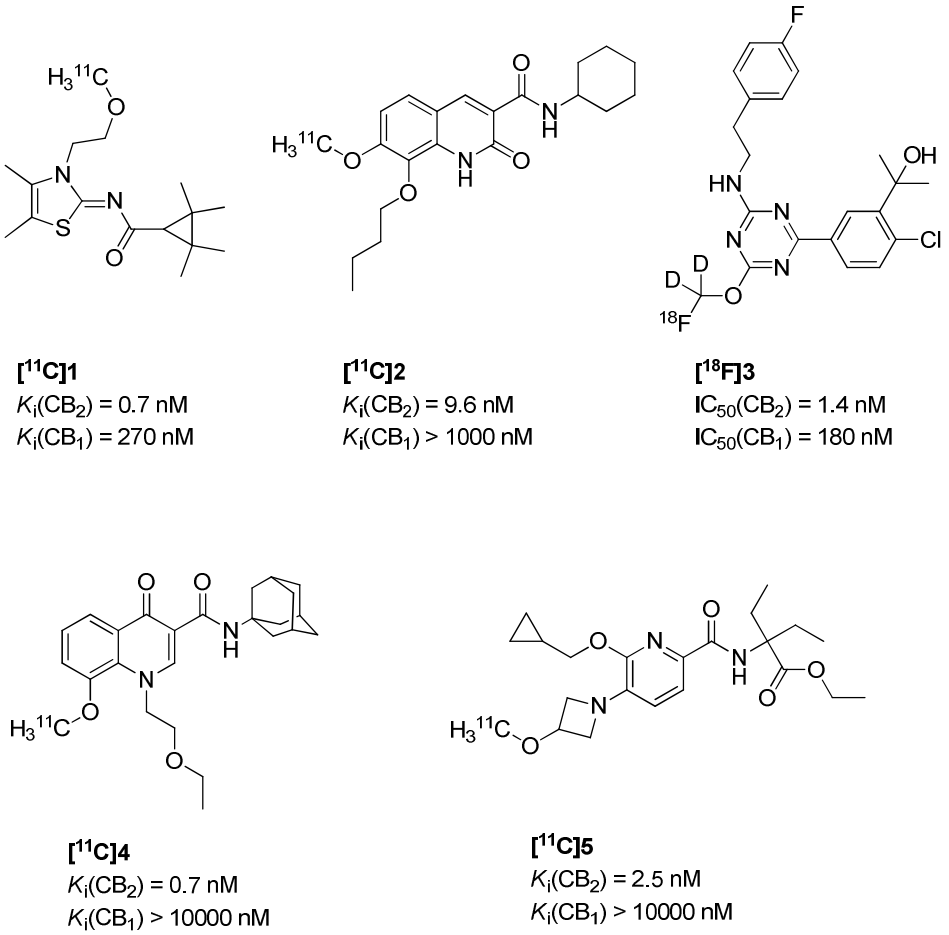

Figure 1. Representative radiolabeled CB_2-ligands.[42, 44, 47, 49,50]

Our aim was to develop an ^{18}F-labeled PET radiotracer based on the scaffold of compound **1**[51] (Figure 2). The newly synthesized derivatives contain the basic structural features of the lead compound **1** with modifications to increase CB_2 binding affinity and selectivity versus CB_1 combined with a facile incorporation of the fluorine-18 ([^{18}F]) *via* nucleophilic substitution at aliphatic position. As part of our efforts, modifications at the thiazole *N*-alkyl chain, thiazole position 5 and at the cyclopropyl subunit were performed (Figure 2 and Table 1) and their impact on CB_2 binding affinity and selectivity towards CB_1 were investigated. Based on the structure-activity relationship findings, radiofluorination and biological investigation in a murine model of neuroinflammation were performed for the most promising derivative.

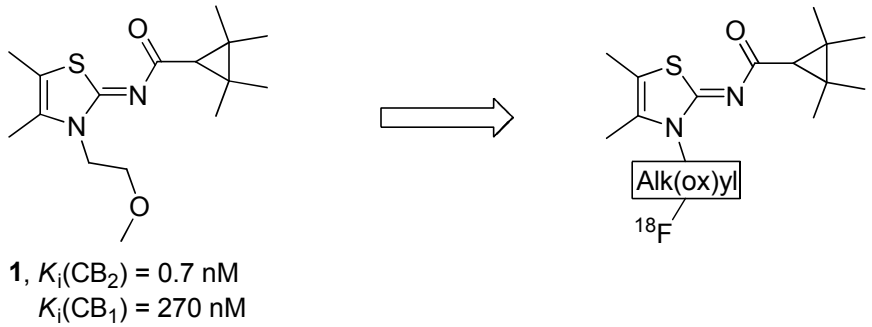

Figure 2. Lead compound **1**[52] and proposed fluoro-derivatization. For details on the Alk(ox)yl see Scheme 1.

RESULTS

Synthesis

The synthesis of the new derivatives has been performed as earlier described for **1**[42] and shown in Scheme 1 with minor modifications. Generally, the synthesis is starting with the commercially available thiazole **6** as free base which is *N*-alkylated in solvent free, thermal reactions conditions followed by the BOP reagent mediated coupling with 2,2,3,3-tetramethyl-cyclopropylcarboxylic acid to give compounds **17**-**29** (Scheme 1).

For the synthesis of the fluoro-triethylene and fluoro-tetraethylene glycols **20** and **21** (see Scheme 1) tosylates **34** and **35** were synthesized as shown in Scheme 2. Triethylene and tetraethylene glycol (**30** and **31** respectively) were bitosylated then monofluorinated using TBAF resulting in a 42% yield over two steps (Scheme 2A).[53, 54] The commercially available 2-amine-4,5-dimethylthiazol (**6**) was reacted with the two corresponding tosylates **34** and **35** (Scheme 2) in a minimum amount of DMF (to solubilize) to provide compounds **7** and **8** respectively as -OTs salts as observed by 1H NMR spectroscopy (Scheme 1).

For the synthesis of the compounds **25** and **26** (Scheme 1), mesylates **37** and **40** respectively, were synthesized as racemates from the corresponding alcohols (Scheme 2B and C).[55] All the other *N*-alkylating agents used for the synthesis of compounds **7-16** (Scheme 1) were commercially available. The coupling of derivatives **7-16** with 2,2,3,3-tetramethyl-cyclopropylcarboxylic acid was performed according to the general procedure previously described,[42] by employing BOP as coupling reagent and triethylamine (Et_3N) in DCM. Yields between 20 and 45% were obtained. Compounds **18** and **19** were synthesized from the alcohol **17** by Williamson ether synthesis. Analogously, compounds **23** and **24** were synthesized from alcohol **22** (Scheme 1).

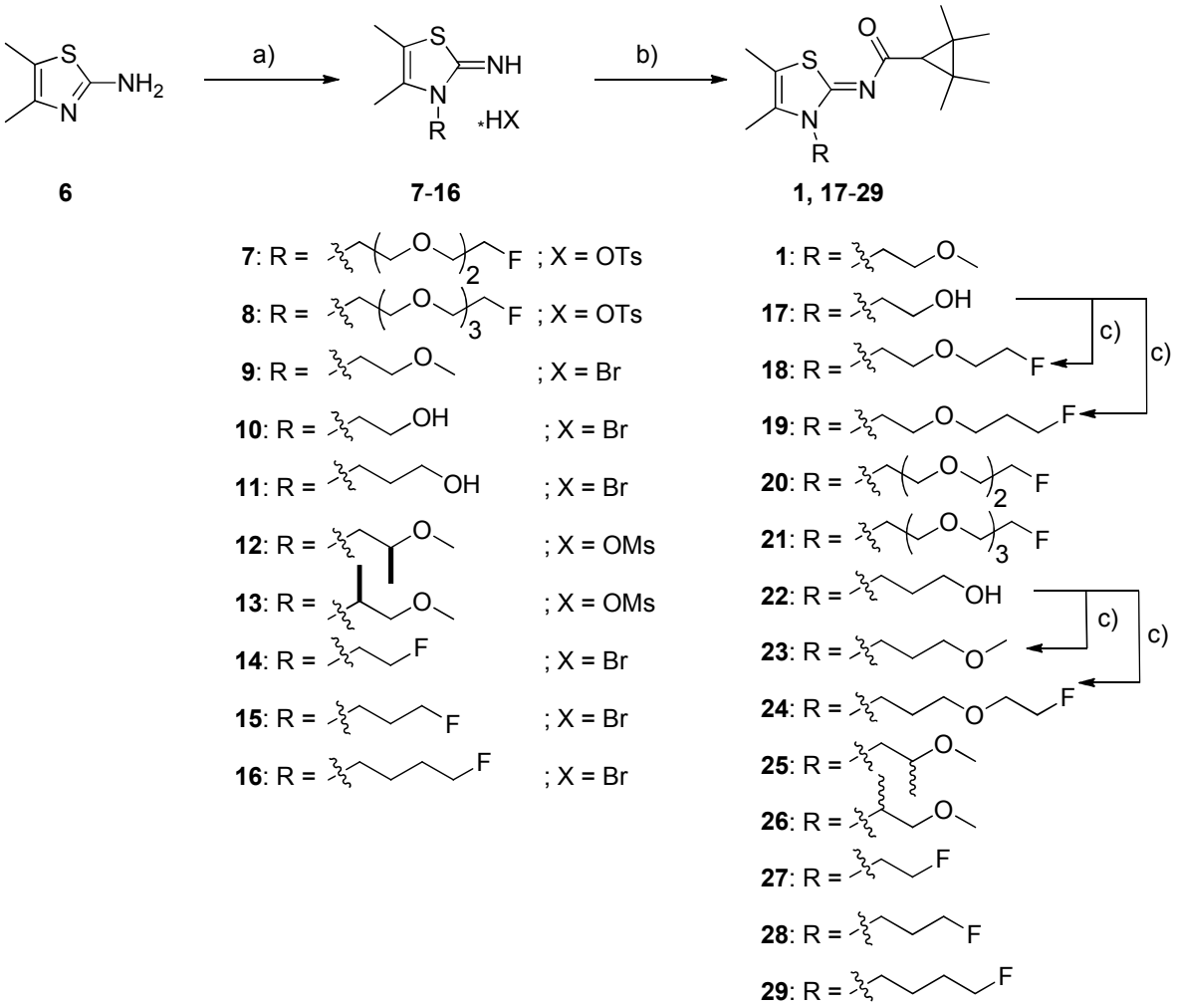

Scheme 1. Synthesis of the lead compound **1** and *N*-alkyl derivatives **17-29**. a) RX, neat, 90 °C, 16 h; b) 2,2,3,3-tetramethylcyclopropane-1-carboxylic acid, BOP, Et_3N, DCM, rt, 24 h, 30-50% over two steps;[42] c) NaH, alkyl bromide, DMF, 0 °C to rt, 80-85%; BOP = (Benzotriazol-1-yloxy)tris(dimethylamino)phosphonium hexafluorophosphate.

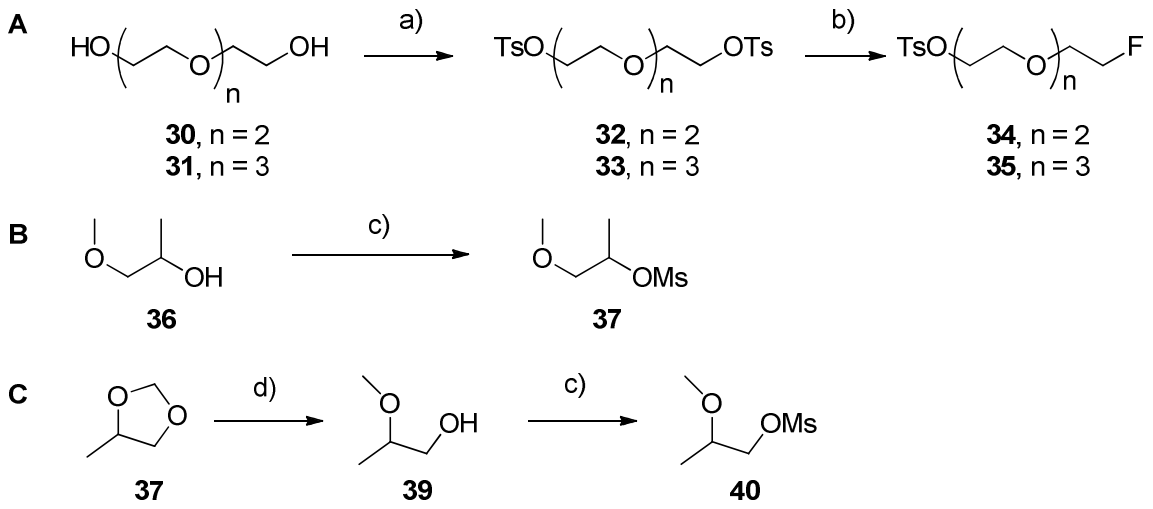

Scheme 2. Synthesis of reagents **34**, **35**, **37** and **40**. a) TsCl, KOH, DCM, 0 °C, 3 h, quantitative;[53] b) TBAF, THF, rt, 16 h, 42%; c) MsCl, Et_3N, DCM, 0 °C to rt, 1 h, quantitative;[56] d) BBr_3, $LiAlH_4$, DCM, 0 °C to rt, 1 h, 90%.[55]

In a further effort to investigate the pharmacology of the lead compound **1**, we introduced a hydroxyl group and its corresponding methyl ether by substituting the 2,2,3,3-tetramethylcyclopropyl partial structure with a 3-(hydroxymethyl)-2,2-dimethylcyclopropyl subunit (compounds **44** and **45** respectively, Scheme 3).

The synthesis of **45** started from the commercially available *rac*-ethyl-chrysanthemate (**41**) which was first oxidized with $KMnO_4$ and the resulting carboxylic acid (**42**, mixture of *cis-trans* isomers)[57] was coupled with the 2-aminothiazole derivative **9** in presence of BOP and Et_3N to

give ester **43**. At this step, epimerization took place presumably *via* Et_3N-mediated deprotonation-protonation at the cyclopropyl subunit. Compound **43** was obtained as a racemic mixture of *trans*-isomers, as determined by 2D-NOESY NMR (see Supporting Information). Reduction of the ester **43** to the alcohol **44** was performed with $LiAlH_4$ in quantitative yield, which was further etherified with MeI under deprotonation *via* Williamson ether synthesis to give **45** in 95% yield over two steps.

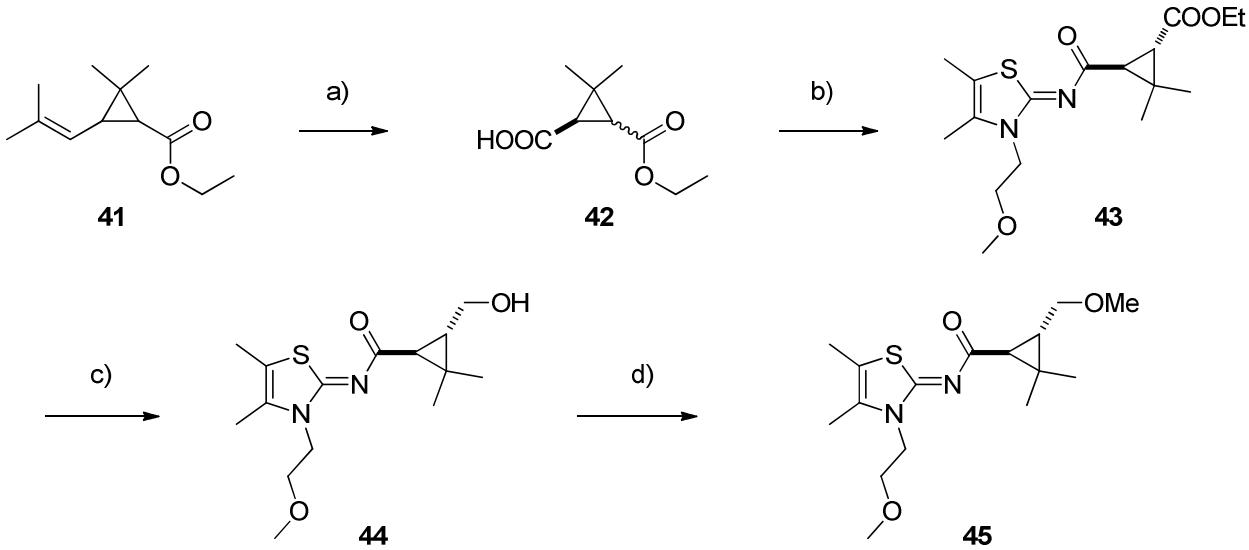

Scheme 3. Synthesis of the hydrophilic derivatives **44** and **45**. a) $KMnO_4$, Na_2SO_3, H_2SO_4, 4 h, 30%;[57] b) **2**, BOP, Et_3N, DCM, rt, 24 h, 42%; c) $LiAlH_4$, THF, rt, 4 h, quantitative; d) NaH, MeI, DMF, 0 °C to rt, 4 h, 95%.

The structure of **1** was also modified at the thiazole 5-position starting from ethyl 3-oxobutanoate which was brominated in the first step[58] and then cyclized with thiourea (Scheme 4). 2-Aminothiazole **48** was *N*-alkylated with 2-bromoethyl methyl ether and then coupled with 2,2,3,3-tetramethylcyclopropane-1-carboxylic to give compound **49**. Double methylation of **49** with the Grignard reagent MeLi gave the 2-isopropanole derivative **50**. Methoxylation of **50** was performed *via* Williamson ether synthesis to form **51** in 79% yield.

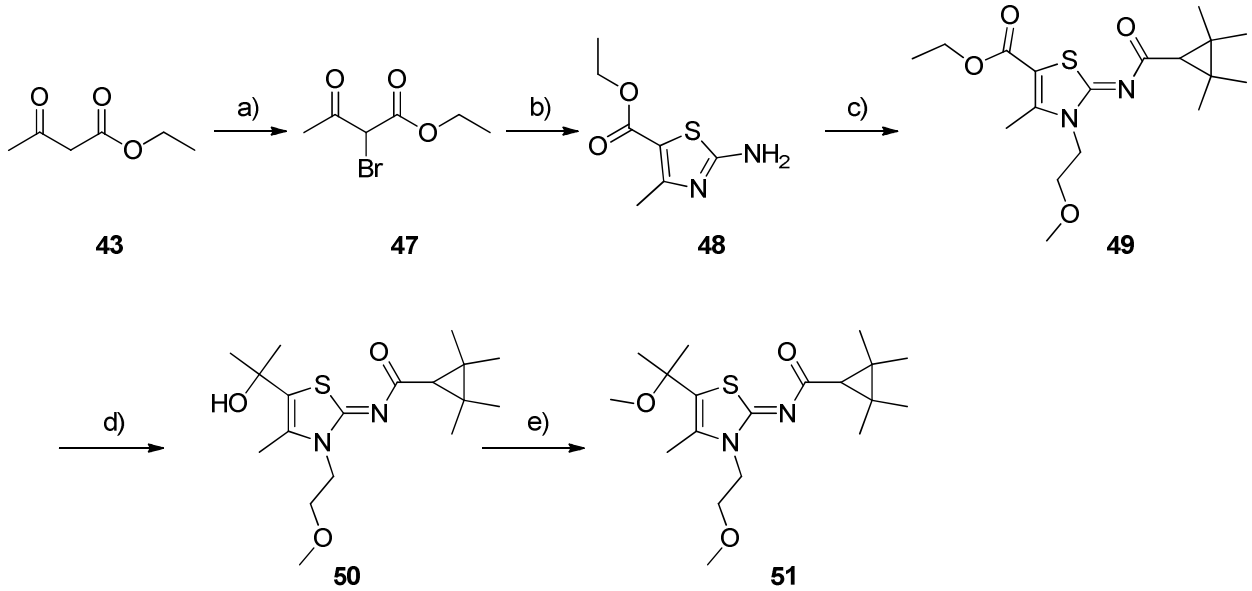

Scheme 4. Synthesis of compounds **50** and **51**. a) KBr, H_2O_2, 1 h, quantitative;[58] b) thiourea, EtOH, reflux, 1 h, quantitative; c) i. 2-Bromoethyl methyl ether, 95 °C, 16 h, ii. 2,2,3,3-tetramethylcyclopropane-1-carboxylic acid, BOP, Et_3N, DCM, rt, 24 h, 36% over two steps; d) MeLi, –78 °C, 30 min, 72%; e) NaH, MeI, overnight, rt, 79%.

Structure-activity relationship

The main purpose of the study was to develop an [^{18}F]fluoro analog of **1** with greater CB_2 binding affinity. The new fluorinated derivative had to be highly selective for CB_2 versus CB_1 (CB_2/CB_1>100) because of the high CB_1 receptor density in the healthy human brain. We mainly focused on compounds **1** *N*-alkyl chain modifications. The binding affinities of the new derivatives were determined by CEREP (France) and HZDR-(Leipzig).

The first *N*-alkyl chain analog of **1** is the fluoro-ethoxyethane derivative **18** that exhibits greater CB_2 binding affinity than **1**, but its CB_2/CB_1 selectivity was reduced (<100 fold) (Table

1). The increase in the number of ethoxyethane groups (**20** and **21**) led to a dramatic reduction in the CB_2 affinity (19 and 1100 nM respectively) compared to **18** and **1** (Table 1).

The propoxyethane analogs of **1** and **18** (compounds **22**, **23** and **24**) exhibited comparable CB_2 and CB_1 binding affinities, but they were slightly more lipophilic. Two derivatives were synthesized by branching a methyl group at the *N*-alkyl chain (compounds **25** and **26**), which led to a significant decrease in the CB_2 binding affinity.

Three further derivatives have been synthesized, **27**, **28** and **29**, all of them lacking the oxygen atom at the thiazole-*N*-alkyl chain subunit and clearly showing the correlation between the thiazole-*N*-alkyl chain length and the binding affinity towards CB_2. Furthermore, derivatization at both the cyclopropyl and thiazole-5-position led to decreased CB_2 binding affinity (compounds **44**, **45** and **50**, Table 1).

Of this new series of compounds (Table 1), **29** manifests the best combination of high CB_2 binding affinity (K_i = 0.39 nM) and excellent CB_2/CB_1 selectivity. It was selected for radiolabeling and animal experiments.

Table 1. Binding affinities of **1** and the new derivatives determined by (A) CEREP (France); (B) HZDR (Leipzig).

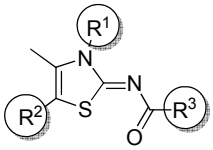	R^1	R^2	R^3	K_iCB_2 (nM)		K_iCB_1 (nM)	
				A	**B**	**A**	**B**
1	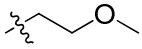	Me		1.2	1.8	270	N/A
18	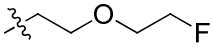	Me		0.31	N/A	25	N/A
19	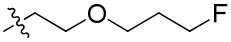	Me		0.70	1.2	33	N/A

20	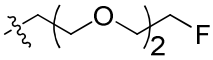	Me		19	12.3	N/A	N/A
21	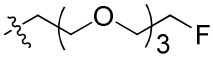	Me		1100	1395	N/A	N/A
23	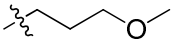	Me		0.81	1.4	N/A	N/A
24	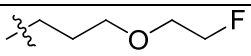	Me		0.94	N/A	N/A	146
25	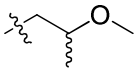	Me		7.0	6.9	N/A	N/A
26	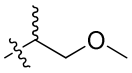	Me		95	212	N/A	N/A
27	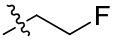	Me		7.2	N/A	N/A	N/A
28	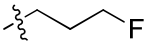	Me		1.2	1.1	1600	N/A
29	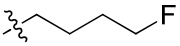	Me		0.39	0.90	380	3031
44	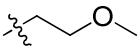	Me	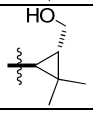	200	N/A	N/A	N/A
45	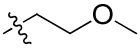	Me	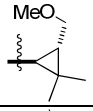	22	53	N/A	N/A
50	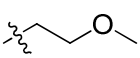			18	N/A	N/A	N/A

N/A = not available.

Radiochemistry

The synthesis of the precursor for the ^{18}F-radiosynthesis (**53**) was performed starting from 4,5-dimethylthiazol-2-amine (**6**) by coupling with 2,2,3,3-tetramethylcyclopropane-1-carboxylic acid in presence of BOP reagent with a 18% yield. Alkylation of the thiazole **52** was performed by using a large excess of 1,4-dibromobutane (10 equiv) and deprotonation with NaH (2 equiv).

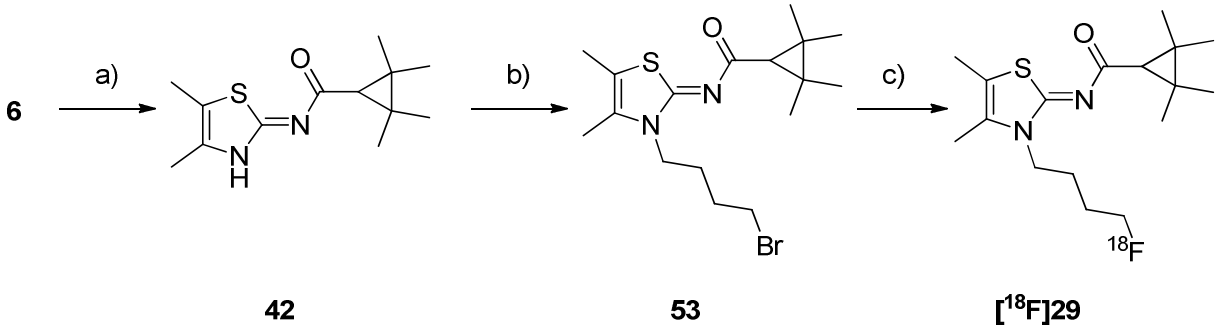

Scheme 5. Synthesis of the precursor for radiolabeling **53** and radiosynthesis of [^{18}F]**29**. a) 2,2,3,3-tetramethylcyclopropane-1-carboxylic acid, BOP, Et_3N, DCM, rt, 24 h, 18%; b) NaH, $Br(CH_2)_4Br$, DMF, rt, overnight, 56%; c) [^{18}F]F-K2.2.2., CH_3CN, 80 °C.

Radiosynthesis of [^{18}F]**29** was achieved by aliphatic nucleophilic substitution of the corresponding bromo precursor (**53**). Manual optimization of the radiosynthesis was performed in order to select the best radiolabeling conditions prior to the transfer to an automated module (e.g. solvent, temperature, heating method and amount of precursor for radiolabeling).

Low labeling yields (≤10%) were obtained when using DMF and DMSO (120-150 °C) as solvents under conventional and microwave-assisted radiofluorination (power cycling mode, 100 W, 120-150 °C) heating methods in presence of the reactive anhydrous K_2CO_3/K2.2.2. complex, which is probably due to the observed decomposition of the bromo precursor **53** at short reaction times (≤ 5 min). No significant increases in labeling efficiencies were noticed when a two-fold increase of precursor amount was used with DMF and DMSO as solvents. The best bromo-to fluoro displacement was obtained when acetonitrile (CH_3CN) was used as the solvent at 80 °C for 15 minutes (labeling yields ~30%) in the presence of the K_2CO_3/K2.2.2. complex (Scheme 5). It is worth mentioning that under these conditions the maximum [^{18}F]F^- incorporation yield

was reached with 3.5 mg of **53**. The radio-thin-layer chromatography (radio-TLC) and the radio-HPLC findings pointed out that besides the desired radiotracer only unreacted radiofluoride was present in the reaction mixture.

For animal experiments, the radiosynthesis of [^{18}F]**29** was translated to the automated module Tracerlab™ FX_{FN} and the total synthesis time was about 70 min (Scheme 5). For isolation of the product, the reaction mixture was transferred onto a semi-preparative HPLC column (entry 7, Figure 3) followed by purification on a pre-conditioned Sep-Pack® C18 light cartridge (entry 11) using EtOH as eluent. An injectable solution was obtained by evaporation of the solvent under a gentle stream of nitrogen at 70 °C with a subsequent addition of a saline-alcohol mixture (0.9%:10% NaCl:EtOH). [^{18}F]**29** was obtained with a 16 ± 8.7% radiochemical yield, high radiochemical purity (≥98%) and a specific activity of 169.7 ± 11.7 GBq/µmol at the end of the synthesis. The identity of [^{18}F]**29** was confirmed by co-injection of the corresponding reference compound as depicted in Figure 4B. *In vitro* evaluation of stability proved that [^{18}F]**29** was stable in saline and EtOH with more than 98% intact radiotracer remaining up to 90 min. An experimental $\log D_{7,4}$ of 3.22 ± 0.03 was found for [^{18}F]**29**, which is within the desired range for compounds that will penetrate the blood-brain barrier.

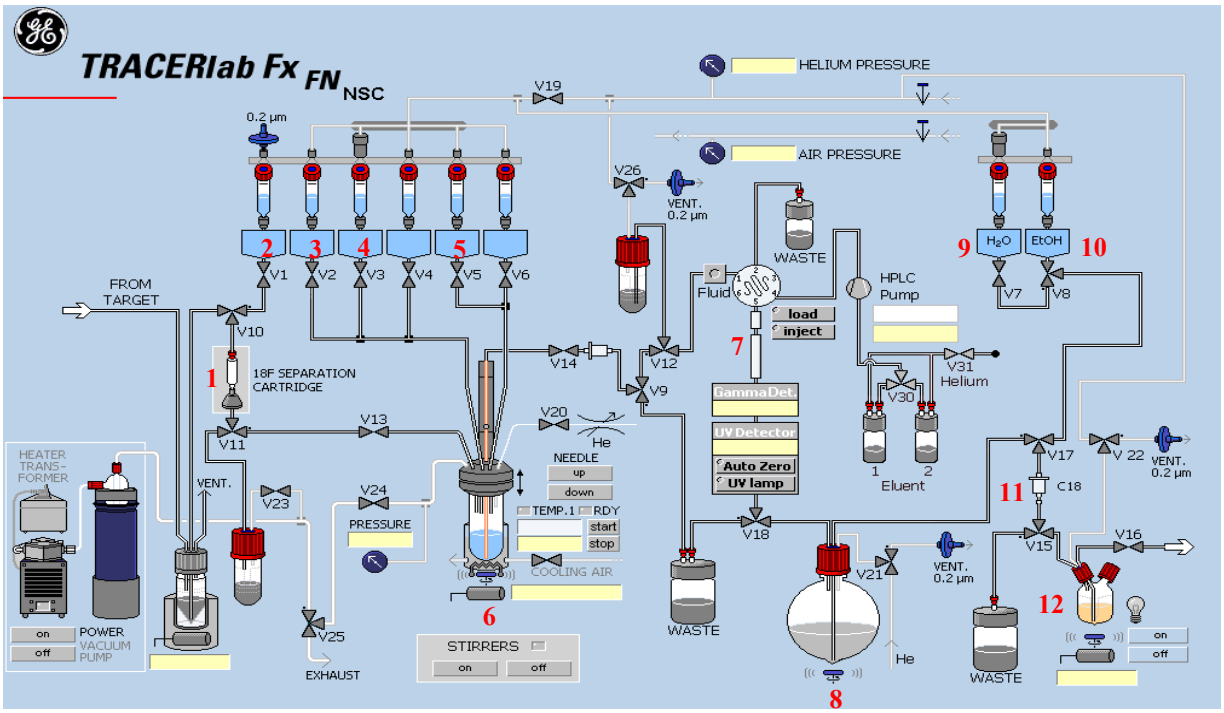

Figure 3. Scheme of the synthesis module Tracer Lab™ FX-FN for the automated radiosynthesis of [^{18}F]**29**. (1) Chromafix® 30 PS-HCO_3^-; (2) K_2CO_3 (1.78 mg in 0.4 mL H_2O); (3) K2.2.2. (11.2 mg in 1 mL CH_3CN); (4) 3.5 mg **53** in 1 mL CH_3CN; (5) 3 mL H_2O/CH_3CN (1:1); (6) Reactor; (7) Reprosil-Pur C18-AQ (65% CH_3CN/20 mM NH_4OAc; flow rate 4.2 mL/min); (8) 40 mL H_2O; (9) 2 mL H_2O; (10) 1.25 mL EtOH; (11) Sep Pak® C18 light cartridge; (12) Product in NaCl 0.9% containing 10% EtOH.

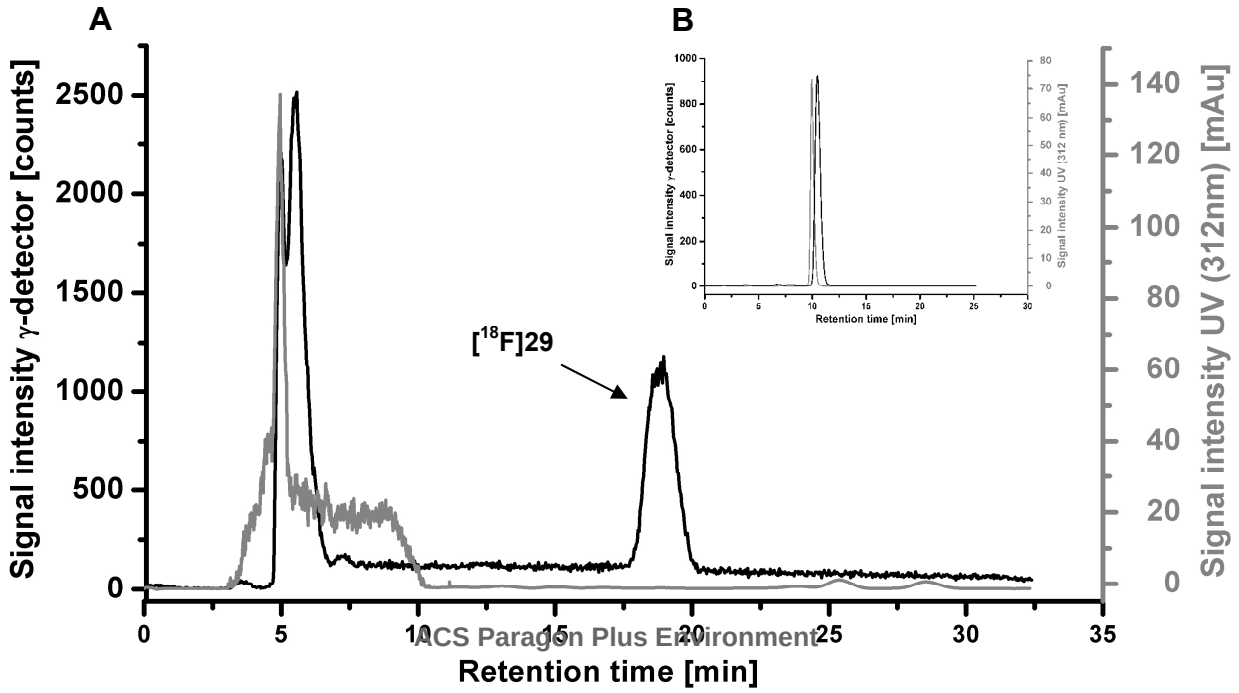

Figure 4. (A) Representative semi-preparative radio-HPLC profile of [^{18}F]**29** (Conditions: Reprosil-Pur 120 C18-AQ (5 µm, 250x10 mm), 65% CH_3CN/20 mM NH_4OAc aq., 4.2 mL/min); (B) Analytical UV- and radio-HPLC chromatogram of [^{18}F]**29** spiked with the corresponding reference compound **29** (conditions: Reprosil-Pur C18-AQ (5 µm, 250x4.6 mm), 70% CH_3CN/20 mM NH_4OAc aq., 1 mL/min). [(solid line, ɣ-trace);(grey line, UV-trace)].

***In vitro* autoradiography studies: radiotracer characterization**

[^{18}F]**29** was further evaluated *in vitro* by receptor autoradiography using rat spleen, an organ which expresses high levels of CB_2 under physiological conditions.[59] For a displacement study, tissue slices were incubated with [^{18}F]**29** without or with the CB_2-selective inverse agonist *N*-[(1*S*)-endo-1,3,3-trimethylbicyclo [2.2.1]-heptane-2-yl]-5-(4-chloro-3-methylphenyl)-1-[(4-methylphenyl)methyl]-1*H*-pyrazole-3-carboxamide (SR144528, **54**), the CB_1-selective antagonist *N*-(piperidin-1-yl)-5-(4-chlorophenyl)-1-(2,4-dichlorophenyl)-4-methyl-1*H*-pyrazole-3-carboxamide (SR141716A, **55**) the CB_1/CB_2-selective agonist (–)-*cis*-3-[2-hydroxy-4-(1,1-dimethylheptyl)phenyl]-*trans*-4-(3-hydroxypropyl)cyclohexanol (CP55,940, **56**) or the non-labelled reference compound **29**. The autoradiograms of the binding of [^{18}F]**29** without and with 1 µM of the indicated compounds are presented in Figure 5A.

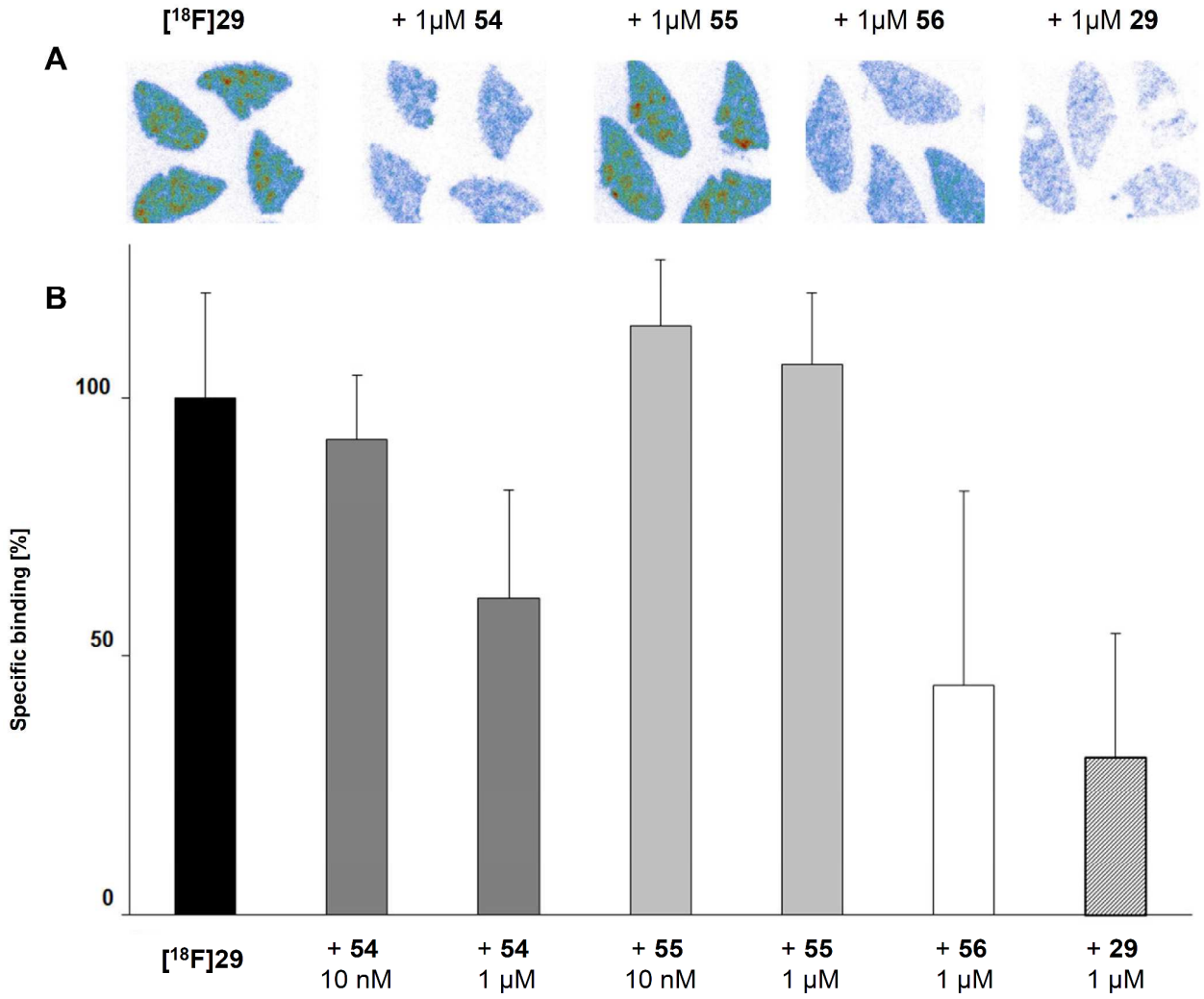

Figure 5. [^{18}F]**29** selectively binds to CB_2 receptors *in vitro*. (A) Rat spleen autoradiograms of [^{18}F]**29** without and with co-incubation of the radioligand with 1 μM of CB_2-specific **54**, CB_1-specific **55**, CB_1/CB_2-specific **56**, and **29**; (B) Evaluation of the specific binding and displacement of [^{18}F]**29** on sections of rat spleen determined without and with co-incubation of the radioligand with CB_2-specific **54** at 10 nM and 1 μM, CB_1-specific **55** at 10 nM and 1 μM, CB_1/CB_2-specific **56** at 1 μM, and **29** at 1 μM.

The specific binding of [^{18}F]**29** in wild type spleen (100%) was displaced by the CB_2-selective compounds **54** at 10 nM (-8%) and 1 μM (-39%) as well as 1 μM of **56** (-56%), and the non-

labelled reference compound **29** (-70%), but remained unaffected by co-incubation with CB_1-targeting **55** at 10 nM and 1 µM (114% and 107%, respectively) (Figure 5B).

In vivo metabolism of [^{18}F]29

In vivo metabolism of [^{18}F]**29** in blood plasma and brain tissue was assessed in female CD-1 mice. Blood samples and brain homogenates were obtained at 30 min post radiotracer injection and proteins removed by organic solvent deproteinization. In general, extraction efficiencies of radioactivity higher than 90% were achieved using MeOH/H_2O (9:1, v/v) as the extraction solvent for both tissues.

The radiometabolite analysis of plasma reflects a rapid metabolism of [^{18}F]**29** with only 7% of intact radiotracer accounting for the total plasma activity at 30 min post injection (Figure 6A). Brain homogenates (Figure 6B) revealed that 36% of the extracted radioactivity was attributable to the intact radiotracer.

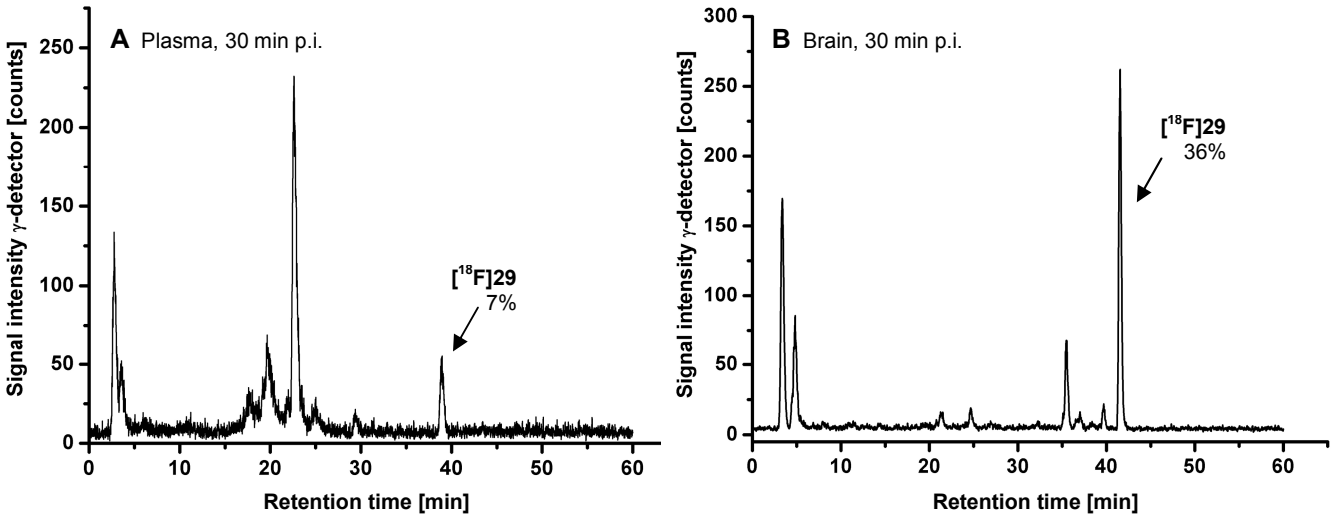

Figure 6. *In vivo* metabolism of [^{18}F]**29** at 30 min p.i.. (A) Plasma samples [Extraction with MeOH/H_2O (9:1); Extraction yield: 94%] and (B) Brain homogenates [Extraction with

MeOH/H_2O (9:1); Extraction yield: 93%]. HPLC conditions: Reprosil-Pur C18-AQ (250x4.6 mm; 5 µm); Gradient mode (10-90% CH_3CN/20 mM NH_4OAc aq.).

PET imaging in healthy CD-1 mice

Dynamic small animal PET/MR scans under baseline conditions were performed in three healthy female CD-1 mice after a bolus i.v. injection of 12.0 ± 4.1 MBq of [^{18}F]**29.** The *in vivo* time-activity curves (TACs) (Figure 7A) reflect high uptake in liver and kidneys followed by a fast washout while the activity concentration is constantly increasing in the intestines, urinary bladder, and gallbladder. The summed whole body PET/MR image (Figure 7B) illustrates these high uptakes for liver and urinary bladder. As region with high CB_2 expression the spleen was investigated separately. The respective TAC (Figure 8A) shows a clear uptake of activity in the spleen (mean SUV, n=3 animals) followed by a washout. In addition, the spleen is visible in the 30 min PET and T1 weighted MR image (Figure 8B). Finally, blocking studies using the CB_2-specific compound **1** were performed to prove the specificity of [^{18}F]**29** towards CB_2. Pre-blocking (3 mg **1**/kg i.p. at 15 min before tracer administration and PET start) significantly reduced the uptake of activity in the spleen ($p<0.05$, students *t* test) compared to the baseline conditions (Figure 8C).

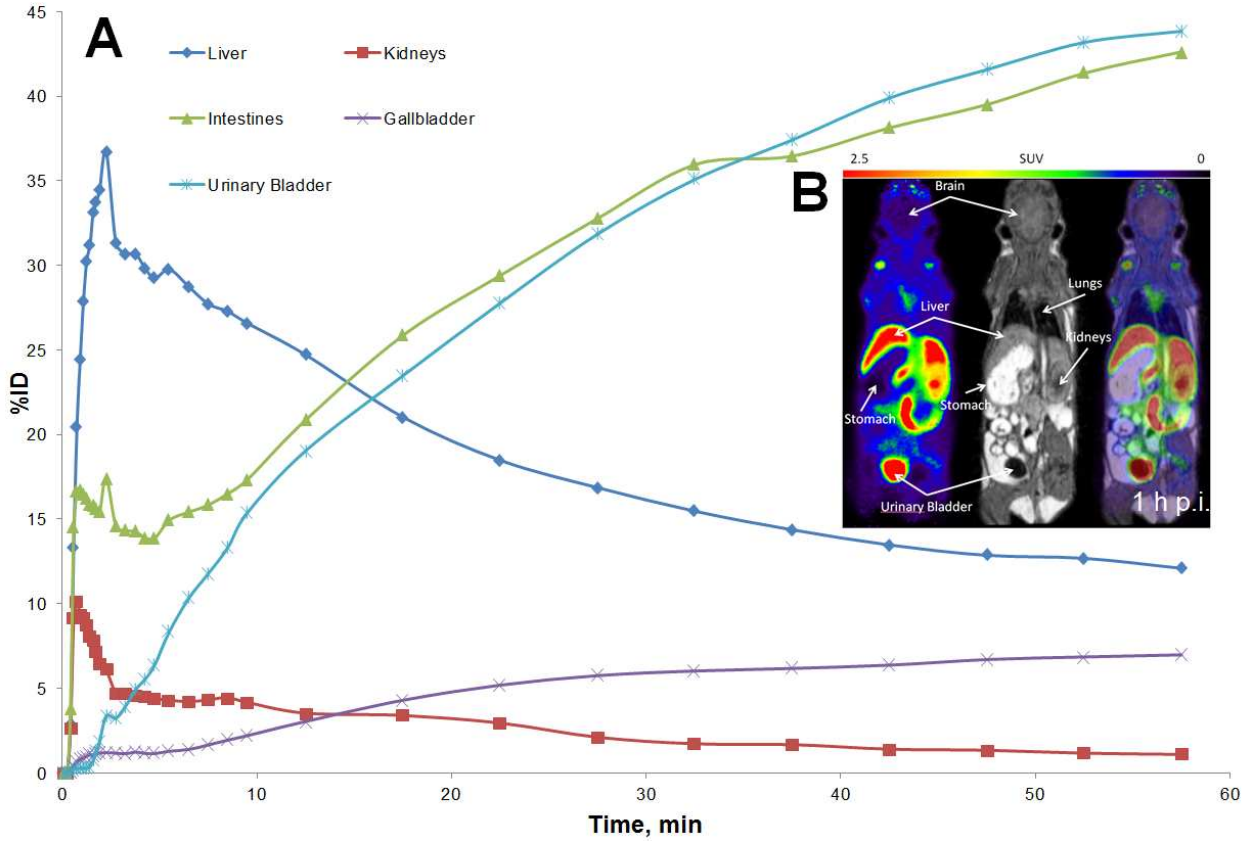

Figure 7. Whole-body pharmacokinetics of [^{18}F]**29**. (A) Small animal PET/MR derived TACs in healthy female CD-1 mice (n=3); (B) Left: Summed whole body PET image (0-60 min p.i.), Middle: T1 weighted whole body MR image, Right: Fused PET/MR images of one representative animal.

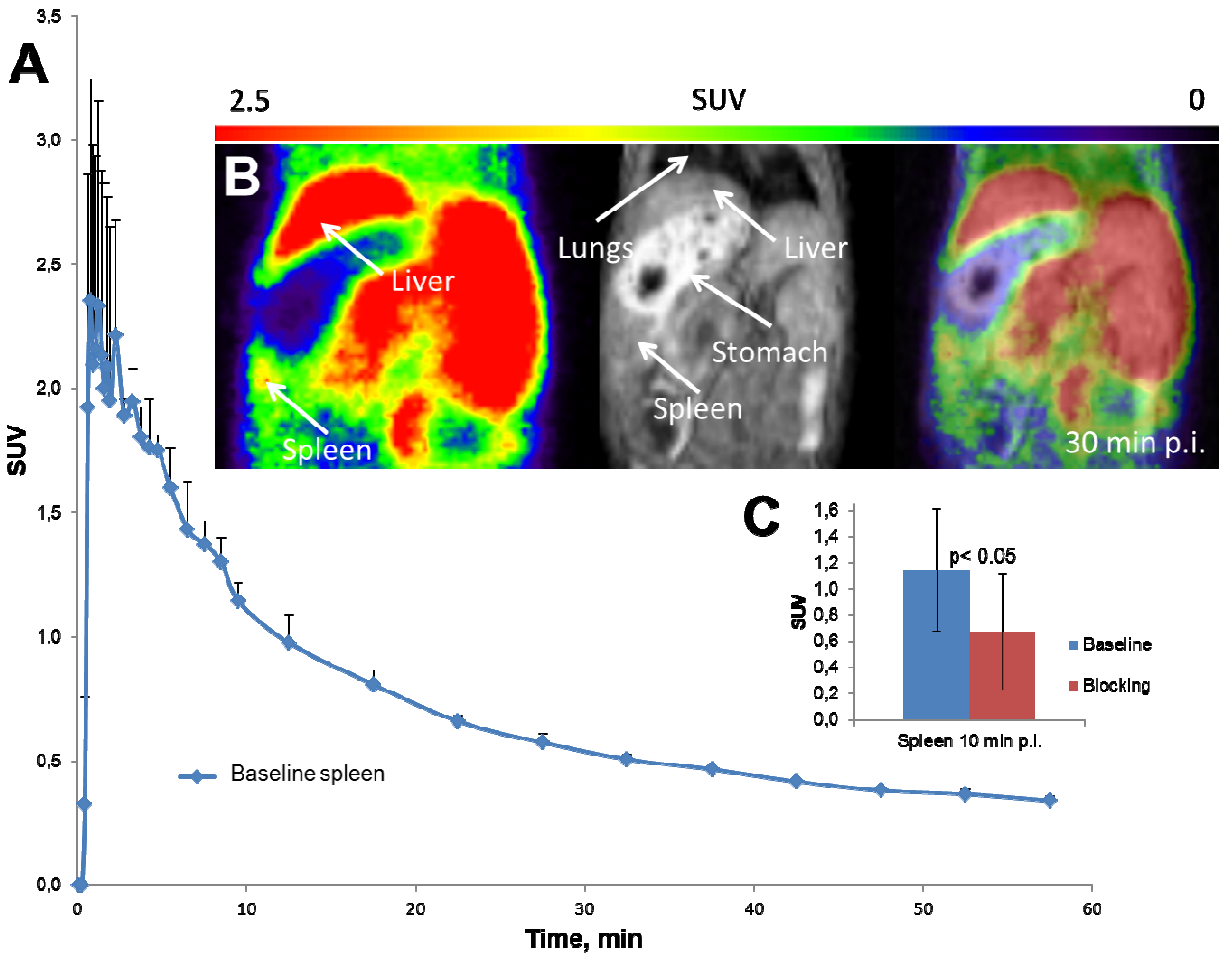

Figure 8. Spleen uptake of [^{18}F]**29** (A) TAC of the spleen showing mean SUV (n=3) and standard deviation; (B) Detailed view of the abdominal region (Left: PET; Middle: T1 weighted MR; Right: PET/MR fusion) with main organs highlighted by arrows; (C) Spleen uptake under baseline and pre-blocking conditions (3 mg/kg **1**, i.p. at 15 min before tracer) . Activity uptake at 10 min p.i. of [^{18}F]**29** is signifcantly reduced by pre-blocking ($p<0.05$, students *t* test) .

PET [^{18}F]29 imaging in a mouse model of neuroinflammation

PET scans with [^{18}F]**29** were performed in a lipopolysaccharide (LPS) mouse model of neuroinflammation. In this model, mice are injected i.p. with 5 mg/kg LPS that result in a rapid increase of brain TNFα that remains activated for a prolonged period of time.[60]

In our study three pairs of mice (LPS-treated and control) were scanned side-by-side after the bolus iv administration of [^{18}F]**29** (7.4 – 11.1 MBq, specific activity >370 GBq/µmol) and time-activity curves (whole brain) were generated (Figure 9A). When comparing the area-under-the-curve (AUC) using the non-parametric Mann-Whitney test (one tailed), a statistically significant difference (p=0.05) was observed between the control and LPS groups. The study demonstrated significantly increased brain uptake of [^{18}F]**29** in the LPS-treated animals versus control animals. In a separate experiment using the same arrangement, the LPS-treated mice were pre-injected with the highly selective CB_2 binding affinity agonist **1** (1 mg/kg, i.p.) and compared to control animals injected with vehicle (Figure 9B). Almost identical average time-activity curves were observed demonstrating no difference between the LPS-treated animals pre-injected with the CB_2 agonist and the control animals. This result further demonstrates that the elevated uptake of [^{18}F]**29** in the LPS-treated animals in the baseline study is specific and mediated by the CB_2 receptor.

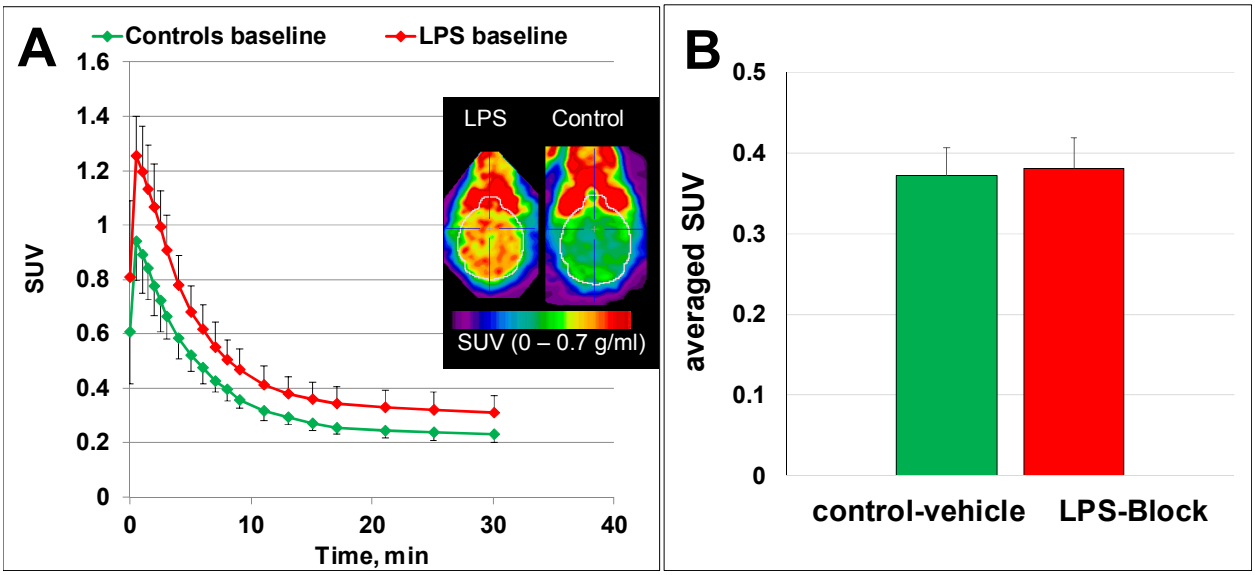

Figure 9. PET whole brain uptake of [^{18}F]**29** in LPS-treated (red) and control (green) mice. (A) Comparison of [^{18}F]**29** baseline uptake in LPS-treated and control mice. There was a statistically

significant difference between the LPS-treated and control animals ($p < 0.05$, non-parametric Mann-Whitney test (one tailed) of the area-under-curve), Data: mean SUV ± SD (n = 3). Insert: representative images of LPS and control mice (0 - 35 min); (B) Whole brain uptake of [^{18}F]**29** in the LPS-treated mice is reduced with injection of CB_2 agonist **1** (solution in 50% aq DMSO, i.p.) to the nearly same level as that in control mice injected with vehicle. Data: averaged (10-30 min) SUV ± SD (n = 3).

DISCUSSION

Our previous studies with [^{11}C]**1** showed the potential of this radioligand to image neuroinflammation-induced increases of CB_2 receptor densities in LPS-treated mice[42] and in a mouse model of Aβ amyloidosis.[43]

To achieve a PET radioligand with a longer half-life for CB_2 receptor imaging in the brain, a new series of **1** derivatives has been synthesized (Scheme 1). First, the influence of the thiazole *N*-alkyl chain length and atomic composition on the CB_2 receptors binding affinity and selectivity against CB_1 receptors was investigated for the possibility to introduce the fluorine atom. Large substituents like the hydrophobic tri- and tetraethylene glycols have been implemented to increase hydrophilicity and also *N*-alkyl ethers which are comparable in size to **1**. The role of the oxygen atom at the *N*-alkyl chain was investigated by shifting its position and also by excluding it in the case of the more lipophilic fluoro-ethyl, -propyl and -butyl derivatives **27**, **28** and **29** respectively.

The *N*-alkylation of the 2-amino-4,5-dimethyl thiazole (Scheme 2) was generally performed at elevated temperatures in sealed tube, neat, except for compounds **7** and **8**, where DMF was used to solubilize the reaction mixture since tosylates **34** and **35** are solid compounds. The resulting

N-alkylated compounds (**7-16**, Scheme 1) were obtained as salts. The amide formation step was mediated by the BOP coupling reagent as earlier described (Scheme 1).[42] In further efforts to functionalize the structure of **1**, modifications at the cyclopropyl and at the thiazole subunit were performed (Scheme 3 and Scheme 4). As a result, alcohols **44** and **50** have been obtained (Scheme 3 and Scheme 4 respectively) which are important key building blocks for further derivatizations at these subunits.

Our structure-activity relationship study shows that implementation of large substituents at the thiazole nitrogen (**20** and **21**) cause a sharp decrease in CB_2 binding affinity. By taking advantage of the *N*-alkyl ether chain of the lead **1**, elongation to ethyl and propyl derivatives (**15** and **19**, respectively) kept the binding affinity while an average 9-fold decrease in selectivity towards CB_1 was observed. Aside from the branched analogs **25** and **26**, a CB_2 binding affinity in the same range as the lead compound (along with a decreased selectivity) was found when the oxygen atom position was changed in the *N*-alkyl chain (**23** and **24**).

Derivatization at both the cyclopropyl and thiazole 5-positions were not well tolerated as reflected by the average 16-fold decrease in binding affinity for the derivatives **45** and **50**. The replacement of the thiazole *N*-methoxyethyl with fluoroalkyl (e.g. fluoro *N*-ethyl (**27**), -propyl (**28**) and -butyl (**29**) derivatives) resulted in a progressive increase in binding affinity and selectivity with the chain length. As a result, the robust subnanomolar affinity of the thiazole *N*-butyl-4-fluoro derivative **29** (CB_2 = 0.39 nM) in combination with the ≥900-fold selectivity towards CB_1 and suitable lipophilicity ($LogD_{7.4}$= 3.22 ± 0.03) lead us to perform the radiosynthesis and biological investigation of [^{18}F]**29**.

The precursor for the radiosynthesis, (compound **53,** Scheme 5) was obtained by first coupling 4,5-dimethylthiazol-2-amine (**6**) with 2,2,3,3-tetramethylcyclopropane-1-carboxylic acid in

presence of BOP reagent followed by deprotonative *N*-alkylation of the thiazole with 1,2-dibromobutane in 10% yield over two steps.

A fully automated radiosynthesis of [^{18}F]**29** was successfully accomplished *via* aliphatic nucleophilic substitution of the corresponding halo precursor **53** in high radiochemical purity (≥98%) and specific activity of up to 1073 GBq/µmol at the end of the synthesis (Scheme 5).

The target specificity of [^{18}F]**29** was further evaluated in autoradiographic studies *in vitro* using CB_2 expressing rat spleen.[8] The distribution pattern of [^{18}F]**29** corresponds with the binding of [^{3}H]**56** in the spleen, which is assumed to detect CB_2-expressing B lymphocytes in the immune system of rats.[59] Blocking experiments with the reference compound **29** and the CB_2-selective inverse agonist **54** confirmed saturable and specific binding of [^{18}F]**29** to CB_2. Plasma and brain samples were investigated at 30 minutes post injection *via* radio-HPLC and a fast metabolism of [^{18}F]**29** *in vivo* was observed. Thus, at this time point ~7% intact [^{18}F]**29** was found in plasma and ~36% in the brain samples.

Small-animal PET/MR experiments were performed in healthy female CD-1 mice to investigate the peripheral pharmacokinetics of [^{18}F]**29**. The studies revealed high uptake in liver, kidneys, intestines, urinary bladder, and gallbladder confirming a hepatic tracer excretion pathway. Furthermore, a clear and marked uptake was found in the spleen as target specific tissue. It could be blocked by the CB_2 selective agonist **1**.

Compound [^{18}F]**29** was studied with micro-PET in both healthy CD-1 mice and a murine neuroinflammation mouse model induced by LPS. An elevated radiotracer uptake in the brain of the LPS-treated mice compared to control was observed. Moreover, blocking experiments performed by pre-injecting the LPS-treated mice with a CB_2 selective ligand proved the CB_2 specificity of the herein described radiotracer.

CONCLUSIONS

A novel series of highly CB_2 affine derivatives of **1** has been developed for PET imaging. Compound **29** demonstrated high CB_2 binding affinity and selectivity, and therefore it was selected for ^{18}F radiolabeling. [^{18}F]**29** was successfully synthesized with high radiochemical purity and specific activities. *In vitro* autoradiography findings using rat spleen as well as *in vivo* small-animal PET/MR imaging confirmed CB_2 specific binding. In addition, small-animal PET studies showed that [^{18}F]**29** readily entered the mouse brain and specifically labeled brain CB_2 receptors in a mouse model of neuroinflammation. Rapid metabolism and the presence of brain-penetrating radiometabolites diminishes the potential of [^{18}F]**29** to image CB_2 receptors with PET.

EXPERIMENTAL

All reagents were used directly as obtained commercially unless otherwise noted. Reaction progress was monitored by thin-layer chromatography (TLC) using silica gel 60 F254 (0.040 − 0.063 mm) with detection by UV. All moisture-sensitive reactions were performed under an argon atmosphere using oven-dried glassware and anhydrous solvents. Column flash chromatography was carried out using E. Merck silica gel 60F (230–400 mesh). Analytical TLC was performed on aluminum sheets coated with silica gel 60 F254 (0.25 mm thickness, E. Merck, Darmstadt, Germany). Melting points were determined with a Fisher-Johns apparatus and were not corrected. ^1H NMR spectra were recorded with a Bruker-400 NMR spectrometer at nominal resonance frequencies of 400 MHz, in $CDCl_3$ or DMSO-d_6 (referenced to internal Me_4Si at δH 0 ppm). The chemical shifts (δ) were expressed in parts per million (ppm). High resolution

mass spectra were recorded utilizing electrospray ionization (ESI) at the University of Notre Dame Mass Spectrometry facility. All compounds that were tested in the biological assays were analyzed by combustion analysis (CHN) to confirm a purity of >95%. Elemental analyses were determined by Galbraith Laboratories (Knoxville, TN). A dose calibrator (Capintec 15R) was used for all radioactivity measurements. Radiofluorination was performed with a modified GE MicroLab radiochemistry box. The experimental animal protocols were approved by the Animal Care and Use Committee of the Johns Hopkins Medical Institutions and by the respective State of Saxony Animal Care and Use Committee in accordance with the German Law for the Protection of Animals and the EU directive 2010/63/EU.

Chemistry

General procedure 1. 2-amino-4,5-dimethylthiazole (**2**, 1 equiv) and appropriate alkyl-bromide, -mesylate or -tosylate (see Scheme 2, 1.5 equiv) were reacted in a sealed vessel at 90 °C for 16 hours. The resulting residue was triturated with minimum amount of *i*-PrOH, the solid was filtered, dried under high vacuum, and used in the next step without further purification. 2,2,3,3-tetramethylcyclopropane acid (1 mmol, 1 equiv), Et_3N (3 mmol, 3 equiv) and BOP (1.3 mmol, 1.3 equiv) were added to a suspension of the alkylated 2-aminoimidazole (1 mmol, 1 equiv) in 5 mL DCM at 0 °C, and the mixture was stirred at room temperature for 20 hours. The reaction was quenched by addition of 2 mL water followed by a 10 mL aqueous saturated solution of $NaHCO_3$ and 15 mL EtOAc. The phases were separated and the aqueous phase was washed with 2x10 mL EtOAc. The combined organic fractions were washed with 20 mL brine, dried over $MgSO_4$ and concentrated by rotary evaporation. The obtained residue was purified by

column chromatography (silica, EtOAc:Petrolether, 1/9 to 1/4 for fluorinated and methoxylated derivatives and 2/3 to 1/1 for alcohols).

General procedure 2. NaH was added (60% in mineral oil, 2 mmol, 2 equiv) to a solution of alcohol **17** (1 mmol, 1 equiv), in 0.5 mL DMF, and the mixture was stirred for 5 minutes at room temperature. Thereafter the alkylating agent RX (5 mmol, 5 equiv) was added, and the reaction mixture was stirred overnight at room temperature. The reaction was quenched by addition of H_2O (2 mL), followed by 15 mL aqueous saturated solution $NaHCO_3$ and 20 mL EtOAc while stirring. The phases were separated, the organic phase was washed with 20 mL EtOAc and the combined organic fractions were dried over $MgSO_4$ and concentrated under reduced pressure. The resulting residue was subjected to column chromatography purification (silica, EtOAc:Petrolether, 1/9 to 1/4).

(*Z*)-*N*-(3-(2-(2-Fluoroethoxy)ethyl)-4,5-dimethylthiazol-2(3*H*)-ylidene)-2,2,3,3-tetramethyl-cyclopropanecarboxamide (18), General procedure 1, white solid, 48% yield; ^{1}H NMR (400 MHz, $CDCl_3$): δ (ppm) = 1.22 (s, 6 H), 1.35 (s, 6 H), 1.53 (s, 1 H), 2.16 (s, 3 H), 2.22 (s, 3 H), 3.65 (t, *J*=6.06 Hz, 2 H), 3.72 (t, *J*=5.31 Hz, 2 H), 4.28 (t, *J*=5.31 Hz, 2 H), 4.44 (t, *J*=5.94 Hz, 1 H), 4.56 (t, *J*=5.94 Hz, 1 H); Elemental analysis: C 59.42, H 7.85, N 8.09, calcd. C 59.62, H 7.95, N 8.18

(*Z*)-*N*-(3-(2-(3-Fluoropropoxy)ethyl)-4,5-dimethylthiazol-2(3*H*)-ylidene)-2,2,3,3-tetramethyl-cyclopropanecarboxamide (19), General procedure 1, white solid, 43% yield; ^{1}H NMR (400 MHz, $CDCl_3$): δ (ppm) = 1.22 (s, 6 H), 1.35 (s, 6 H), 1.53 (s, 1 H), 1.83 - 2.02 (m, 2 H), 2.17 (d, *J*=0.76 Hz, 3 H), 2.21 (d, *J*=0.76 Hz, 3 H), 3.54 (t, *J*=6.06 Hz, 2 H), 3.77 (t, *J*=5.31 Hz, 2 H), 4.26 (t, *J*=5.31 Hz, 2 H), 4.43 (t, *J*=5.94 Hz, 1 H), 4.55 (t, *J*=5.94 Hz, 1 H); ^{13}C NMR (100 MHz, $CDCl_3$): δ (ppm) = 11.41, 11.71, 17.00, 24.10, 30.20, 30.63, 30.83, 42.33, 42.35,

46.30, 66.88, 68.49, 80.27, 81.90, 112.61, 128.32, 135.04, 181.49; HRMS (ESI+): *m*/*z* (%) =357.2004, calcd. 357.2012 for $C_{18}H_{30}FN_2O_2S^+$ $[M+H]^+$; Elemental analysis: C 61.09, H 8.14, N 7.31, calcd. C 60.64, H 8.20, N 7.86

(*Z*)-*N*-(3-(2-(2-(2-Fluoroethoxy)ethoxy)ethyl)-4,5-dimethylthiazol-2(3*H*)-ylidene)-2,2,3,3-tetramethyl-cyclopropanecarboxamide (20), General procedure 1, white solid, 30% yield; ^{1}H NMR (400 MHz, $CDCl_3$): δ (ppm) = 1.22 (s, 6 H), 1.35 (s, 6 H), 1.53 (s, 1 H), 2.16 (d, *J*=0.76 Hz, 3 H), 2.22 (d, *J*=1.01 Hz, 3 H), 3.58 - 3.64 (m, 4 H), 3.64 - 3.67 (m, 1 H), 3.70 - 3.78 (m, 1 H), 3.82 (t, *J*=5.31 Hz, 2 H), 4.27 (t, *J*=5.31 Hz, 2 H), 4.46 - 4.51 (m, 1 H), 4.56 - 4.66 (m, 1 H); ^{13}C NMR (100 MHz, $CDCl_3$): δ (ppm) = 11.43, 11.70, 17.00 (2 C), 24.11, 30.19, 42.32, 46.27, 68.72, 70.27, 70.46, 70.57, 70.75, 82.28, 83.96, 112.50, 128.51, 164.37, 181.45; HRMS (ESI+): *m*/*z* (%) = 387.2127, calcd. 387.2118 for $C_{19}H_{32}FN_2O_3S^+$ $[M+H]^+$; Elemental analysis: C 59.53, H 8.14, N 6.93, calcd. C 59.04, H 8.08, N 7.25

(*Z*)-*N*-(3-(2-(2-(2-(2-Fluoroethoxy)ethoxy)ethoxy)ethyl)-4,5-dimethylthiazol-2(3*H*)-ylidene)-2,2,3,3-tetramethyl-cyclopropanecarboxamide (21), General procedure 1, white solid, 30% yield; ^{1}H NMR (400 MHz, $CDCl_3$): δ (ppm) = 1.22 (s, 6 H), 1.34 (s, 6 H), 1.53 (s, 1 H), 2.16 (d, *J*=1.01 Hz, 3 H), 2.22 (d, *J*=1.01 Hz, 3 H), 3.54 - 3.76 (m, 9 H), 3.76 - 3.86 (m, 3 H), 4.26 (t, *J*=5.43 Hz, 2 H), 4.47 - 4.55 (m, 1 H), 4.58 - 4.68 (m, 1 H); ^{13}C NMR (100 MHz, $CDCl_3$): δ (ppm) =11.46, 11.72, 17.01, 24.12 (4 C), 30.20, 42.32, 46.30, 68.71, 70.53, 70.61, 70.65, 70.84, 82.33, 84.01, 114.53, 127.26, 165.13, 181.10; HRMS (ESI+): *m*/*z* (%) = 431.2392, calcd. 431.2380 for $C_{21}H_{36}FN_2O_4S^+$ $[M+H]^+$; Elemental analysis: C 58.44, H 8.19, N, 6.71, calcd. C 58.58, H 8.19, N 6.51

(*Z*)-*N*-(3-(3-Hydroxypropyl)-4,5-dimethylthiazol-2(3*H*)-ylidene)-2,2,3,3-tetramethyl-cyclopropanecarboxamide (22), General procedure 1, white solid, 39% yield; ^{1}H NMR (400

MHz, $CDCl_3$): δ (ppm) = 1.21 (s, 7 H), 1.31 (s, 6 H), 1.45 (s, 1 H), 1.76 - 1.95 (m, 2 H), 2.18 (d, *J*=0.76 Hz, 3 H), 2.21 (d, *J*=1.01 Hz, 3 H), 3.39 - 3.49 (m, 2 H), 4.24 - 4.36 (m, 2 H); ^{13}C NMR (100 MHz, $CDCl_3$): δ (ppm) = 11.01, 11.58, 16.93 (2 C), 23.86 (4 C), 30.48, 32.11 (2 C), 41.91, 42.48, 56.62, 114.64, 127.68, 165.45, 180.57

(*Z*)-*N*-(3-(3-Methoxypropyl)-4,5-dimethylthiazol-2(3*H*)-ylidene)-2,2,3,3-tetramethyl-cyclopropanecarboxamide (23), General procedure 2; white solid, 78% yield; ^{1}H NMR (400 MHz, $CDCl_3$): δ (ppm) = 1.22 (s, 6 H), 1.35 (s, 6 H), 1.55 (s, 1 H), 1.97 - 2.09 (m, 2 H), 2.16 (d, *J*=1.01 Hz, 3 H), 2.19 (d, *J*=0.76 Hz, 3 H), 3.36 (s, 3 H), 3.41 (t, *J*=5.81 Hz, 2 H), 4.14 - 4.23 (m, 2 H); ^{13}C NMR (100 MHz, $CDCl_3$): δ (ppm) =10.96, 11.70, 17.01 (4 C), 24.12, 28.58, 30.12, 42.32, 43.61, 58.61, 69.56, 114.86, 127.65, 164.37, 181.53; HRMS (ESI+): *m*/*z* (%) = 325.1968, calcd. 325.1950 for $C_{17}H_{29}N_2O_2S^+$ $[M+H]^+$; Elemental analysis: C 62.93, H 8.92, N 8.67, calcd. C 62.93, H 8.70, N 8.63

(*Z*)-*N*-(3-(3-(2-Fluoroethoxy)propyl)-4,5-dimethylthiazol-2(3*H*)-ylidene)-2,2,3,3-tetramethyl-cyclopropanecarboxamide (24), General procedure 2, white solid, 65% yield; ^{1}H NMR (400 MHz, $CDCl_3$): δ (ppm) = 1.22 (s, 6 H), 1.35 (s, 6 H), 1.54 (s, 1 H), 2.03 - 2.13 (m, 2 H), 2.17 (s, 3 H), 2.20 (s, 3 H), 3.54 (t, *J*=5.81 Hz, 2 H), 3.66 (dd, *J*=4.67, 3.66 Hz, 1 H), 3.74 (dd, *J*=4.80, 3.54 Hz, 1 H), 4.22 (t, *J*=6.95 Hz, 2 H), 4.47 - 4.56 (m, 1 H), 4.59 - 4.69 (m, 1 H); ^{13}C NMR (100 MHz, $CDCl_3$): δ (ppm) = 10.97, 11.69, 17.00 (4 C), 24.12, 28.57, 30.17, 42.81, 68.31, 69.89, 70.09, 81.52, 100.00, 117.88, 154.02, 183.54; HRMS (ESI+): *m*/*z* (%) = 357.2030, calcd. 357.2012 for $C_{18}H_{30}FN_2O_2S^+$ $[M+H]^+$; Elemental analysis: C 60.77, H 8.26, N 7.74 calcd. C 60.64, H 8.20, N 7.86

(*Z*)-*N*-(3-(2-Methoxypropyl)-4,5-dimethylthiazol-2(3*H*)-ylidene)-2,2,3,3-tetramethyl-cyclopropanecarboxamide (25), General procedure 1, white solid, 35% yield; ^{1}H NMR (400

MHz, $CDCl_3$): δ (ppm) = 1.25 (d, *J*=3.40 Hz, 6 H), 1.33 (s, 3 H), 1.36 (s, 3 H), 1.52 (s, 1 H), 2.16 (d, *J*=0.76 Hz, 3 H), 2.20 (d, *J*=0.76 Hz, 3 H), 3.23 (s, 3 H), 3.73 - 3.83 (m, 1 H), 3.83 - 3.93 (m, 1 H), 4.24 (dd, *J*=13.39, 3.28 Hz, 1 H); ^{13}C NMR (100 MHz, $CDCl_3$): δ (ppm) = 11.63, 17.04, 17.06, 17.10 (2 C), 24.09, 24.15, 29.93, 30.05, 42.37, 51.79, 57.00, 74.89, 112.39, 128.75, 164.46, 181.44; HRMS (ESI+): *m*/*z* (%) = 325.1962 calcd. 325.1950 for $C_{17}H_{29}N_2O_2S^+$ $[M+H]^+$; Elemental analysis: C 62.23, H 8.59, N 8.26, calcd. C 62.93, H 8.70, N 8.63

(*Z*)-*N*-(3-(1-Methoxypropan-2-yl)-4,5-dimethylthiazol-2(3*H*)-ylidene)-2,2,3,3-tetramethyl-cyclopropanecarboxamide (26), General procedure 1, white solid, 38% yield; ^{1}H NMR (400 MHz, $CDCl_3$): δ (ppm) = 1.21 (d, *J*=3.40 Hz, 3 H), 1.34 (s, 6 H), 1.52 (s, 1 H), 2.14 (s, 3 H), 2.17 (s, 3 H), 3.32 (s, 3 H), 3.70 - 3.83 (m, 1 H), 4.20 – 4.60 (m, 2H H); ^{13}C NMR (100 MHz, $CDCl_3$): δ (ppm) =12.06, 17.07 (4 C) 24.10 (2 C), 29.86 (2 C), 42.55, 52.19, 59.00, 73.33, 117.07, 128.13, 155.82, 167.82; HRMS (ESI+): *m*/*z* (%) = 325.1980, calcd. 325.1950 for $C_{17}H_{29}N_2O_2S^+$ $[M+H]^+$; Elemental analysis: C 62.30, H 8.72, N 8.25, calcd. C 62.93, H 8.70, N 8.63

(*Z*)-*N*-(3-(2-Fluoroethyl)-4,5-dimethylthiazol-2(3*H*)-ylidene)-2,2,3,3-tetramethyl-cyclopropanecarboxamide (27), General procedure 1, white solid, 42% yield; ^{1}H NMR (400 MHz, $CDCl_3$): δ (ppm) = 1.22 (s, 6 H), 1.34 (s, 6 H), 1.52 (s, 1 H), 2.17 (d, *J*=0.76 Hz, 3 H), 2.20 (s, 3 H), 4.34 (t, *J*=4.55 Hz, 1 H), 4.41 (t, *J*=4.67 Hz, 1 H), 4.72 (t, *J*=4.67 Hz, 1 H),), 4.84 (t, *J*=4.55 Hz, 1 H); ^{13}C NMR (100 MHz, $CDCl_3$): δ (ppm) = 11.35, 11.71, 16.95 (4 C), 24.07, 42.35, 46.46, 46.65, 81.82, 112.93, 127.87, 143.37, 181.48; HRMS (ESI+): *m*/*z* (%) = 299.1604, calcd. 299.1593 for $C_{15}H_{24}FN_2OS^+$ $[M+H]^+$; Elemental analysis: C 60.25, H 7.43, N 9.55, calcd. C 60.37, H 7.77, N 9.39

(*Z*)-*N*-(3-(3-Fluoropropyl)-4,5-dimethylthiazol-2(3*H*)-ylidene)-2,2,3,3-tetramethyl-cyclopropanecarboxamide (28), General procedure 1, white solid, 40% yield; ^{1}H NMR (400 MHz, $CDCl_3$): δ (ppm) = 1.22 (s, 6 H), 1.34 (s, 6 H), 1.54 (s, 1 H), 2.17 (s, 3 H), 1.14 – 2.27 (m, 2 H), 2.20 (d, *J*=0.76 Hz, 3 H), 4.23 (t, *J*=7.07 Hz, 2 H), 4.45 (t, *J*=5.56 Hz, 1 H), 4.57 (t, *J*=5.56 Hz, 1 H); ^{13}C NMR (100 MHz, $CDCl_3$): δ (ppm) = 10.97, 11.70, 16.98 (4 C), 24.09, 29.25, 30.25, 42.52, 42.67, 81.42, 113.27, 127.40, 143.31, 181.58; HRMS (ESI+): *m*/*z* (%) = 313.1765, calcd. 313.1750 for $C_{16}H_{26}FN_2OS^+$ $[M+H]^+$; Elemental analysis: C 61.85, H 8.09, N 8.33, calcd. C 61.51, H 8.06, N 8.97

(*Z*)-*N*-(3-(4-Fluorobutyl)-4,5-dimethylthiazol-2(3*H*)-ylidene)-2,2,3,3-tetramethyl-cyclopropanecarboxamide (29), General procedure 1, white solid, 35% yield; ^{1}H NMR (400 MHz, $CDCl_3$): δ (ppm) = 1.22 (s, 6 H), 1.35 (s, 6 H), 1.53 (s, 1 H), 1.75 (d, *J*=8.34 Hz, 1 H), 1.79 - 1.93 (m, 3 H), 2.16 (d, *J*=1.01 Hz, 3 H), 2.20 (d, *J*=1.01 Hz, 3 H), 4.10 - 4.20 (m, 2 H), 4.48 (t, *J*=5.81 Hz, 1 H), 4.60 (t, *J*=5.68 Hz, 1 H); ^{13}C NMR (100 MHz, $CDCl_3$): δ (ppm) = 11.06, 11.63, 17.03 (4 C), 24.23, 27.44, 29.59, 30.13, 33.04, 42.35, 44.96, 113.52, 127.09, 164.52, 181.51; HRMS (ESI+): *m*/*z* (%) = 327.1912, calcd. 327.1906 for $C_{17}H_{28}FN_2OS^+$ $[M+H]^+$; Elemental analysis: C 62.43, H 8.25, N 8.73, calcd. C 62.54, H 8.34, N 8.58

Ethyl 3-(3-(2-methoxyethyl)-4,5-dimethylthiazol-2(3*H*)-ylidenecarbamoyl)-2,2-dimethyl-cyclopropanecarboxylate (43), General procedure 1, 42% yield; ^{1}H NMR (400 MHz, $CDCl_3$): δ (ppm) = 1.28 (t, *J*=7.07 Hz, 3 H), 1.35 (s, 6 H), 2.17 (s, 3 H), 2.24 (s, 3 H), 2.36 (d, *J*=5.81 Hz, 1 H), 2.51 (d, *J*=5.56 Hz, 1 H), 3.32 (s, 3 H), 3.69 (t, *J*=4.8 Hz, 2 H), 4.05 - 4.27 (m, 3 H), 4.27 - 4.39 (m, 1 H);^{13}C NMR (100MHz, $CDCl_3$): δ (ppm) = 11.53, 11.78, 14.40, 20.57, 21.01, 31.12, 33.84, 39.84, 46.54, 59.10, 60.38, 70.20, 113.49, 129.16, 165.53, 171.86, 178.08

3-(Hydroxymethyl)-*N*-(3-(2-methoxyethyl)-4,5-dimethylthiazol-2(3*H*)-ylidene)-2,2-dimethyl-cyclopropanecarboxamide (44), **43** (500 mg, 1.4 mmol, 1 equiv) in 10 mL THF was added to a suspension of $LiAlH_4$ (53.6 mg, 1.4 mmol, 1 equiv) in 10 mL THF at 0 °C, and the reaction was stirred at the same temperature for one hour. Saturated aqueous NH_4Cl (20) mL and 20 mL EtOAc were added, the phases were separated, the organic phase was washed once with 20 mL brine, dried over $MgSO_4$ and evaporated under reduced pressure to provide **44** (440 mg, 1.4 mmol) as colorless solid in quantitative yield; ^{1}H NMR (400 MHz, $CDCl_3$): δ (ppm) = 1.27 (s, 3 H), 1.31 (s, 3 H), 1.70 (d, *J*=5.56 Hz, 1 H), 1.87 (ddd, *J*=8.34, 6.69, 5.43 Hz, 1 H), 2.18 (d, *J*=1.01 Hz, 3 H), 2.22 (d, *J*=0.76 Hz, 3 H), 3.32 (s, 3 H), 3.65 (dd, *J*=11.49, 8.46 Hz, 1 H), 3.70 (t, *J*=5.31 Hz, 2 H), 3.82 (dd, *J*=11.50, 6.69 Hz, 1 H), 4.14 - 4.25 (m, 1 H), 4.26 - 4.38 (m, 1 H); ^{13}C NMR (100 MHz, $CDCl_3$): δ (ppm) = 11.51, 11.78, 20.99, 21.77, 27.50, 34.78, 37.78, 46.44, 59.11, 62.82, 70.23, 113.24, 128.89, 165.39, 180.11; HRMS (ESI+): *m*/*z* (%) = 313.1603, calcd. 313.1586 for $C_{15}H_{24}N_2O_3S^+$ $[M+H]^+$; Elemental analysis: C 57.63, H 7.86, N 8.92, calcd. C 57.66, H 7.74, N 8.97

***N*-(3-(2-Methoxyethyl)-4,5-dimethylthiazol-2(3*H*)-ylidene)-3-(methoxymethyl)-2,2-dimethyl-cyclopropanecarboxamide (45)**, General procedure 1, white solid, 42% yield; ^{1}H NMR (400 MHz, $CDCl_3$): δ (ppm) = 1.24 (s, 3 H), 1.31 (s, 3 H), 1.65 (d, *J*=5.56 Hz, 1 H), 1.86 (dt, *J*=8.84, 5.68 Hz, 1 H), 2.18 (s, 3 H), 2.21 (d, *J*=0.76 Hz, 3 H), 3.31 (s, 3 H), 3.37 (s, 3 H), 3.65 (dd, *J*=10.61, 5.81 Hz, 1 H), 3.69 (t, *J*=5.31 Hz, 2 H), 4.14 - 4.25 (m, 1 H), 4.25 - 4.37 (m, 1 H); ^{13}C NMR (100 MHz, $CDCl_3$): δ (ppm) = 11.50, 11.77, 20.81, 21.76, 27.43, 31.66, 37.55, 46.39, 58.21, 59.09, 70.21, 72.14, 113.14, 117.89, 128.80, 180.17; HRMS (ESI+): *m*/*z* (%) = 327.1760 calcd. 327.1742 for $C_{16}H_{27}N_2O_3S^+$ $[M+H]^+$; Elemental analysis: C 59.07, H,8.23, N 8.36, calcd. C 58.87, H,8.03, N 8.58

Ethyl 2-amino-4-methylthiazole-5-carboxylate (**48**), A mixture of ethyl 3-oxobutanoate (**46**, 5 g, 38 mmol, 1 equiv), KBr (23 g, 192 mmol, 5 equiv), 1M HCl (185 mL, 192 mmol, 5 equiv), and 30% aqueous H_2O_2 (86 mL) in 185 mL toluene was stirred at room temperature for one hour. The reaction was quenched by slow addition of saturated aqueous $Na_2S_2O_3$ (250 mL) followed by saturated aqueous $NaHCO_3$. The phases were separated, and the aqueous phase was washed with EtOAc (2x200 mL). The combined organic phase was washed with 400 mL brine, dried over $MgSO_4$ and evaporated under reduced pressure to afford ethyl 2-bromo-3-oxobutanoate (**47**) (8 g, 38 mmol, quantitative) as a colorless liquid. Thiourea (0.5 g, 6.6 mmol, 1 equiv) was added to a solution of **47** (1.6 g, 7.2 mmol, 1.1 equiv) in 10 mL EtOH and the reaction was refluxed for one hour. A white solid was formed during the reaction. Most of the solvent was eliminate under reduced pressure. Thereafter, 20 mL 1N aqueous NaOH was added, the resulting mixture was sonicated and placed at 4 °C overnight. The resulting solid was filtrated, washed with water and cold EtOH and dried to give **48** as free base (1.2 g, white solid, 6.6 mmol, quantitative); ^{1}H NMR (400 MHz, $CDCl_3$): δ (ppm) = 1.34 (t, J=7.20 Hz, 3 H), 2.54 (s, 3 H), 4.28 (q, J=7.16 Hz, 2 H), 5.65 (s, 2 H)

Ethyl 3-(2-methoxyethyl)-4-methyl-2-(2,2,3,3-tetramethyl-cyclopropanecarbonylimino)-2,3-dihydrothiazole-5-carboxylate (49), was obtained as white solid, according to general procedure 1 in 36% yield over two steps;^{1}H NMR (400 MHz, $CDCl_3$): δ (ppm) = 1.24 (s, 6 H), 1.31 - 1.35 (m, 3 H), 1.35 - 1.36 (s, 6 H), 1.60 (s, 1 H), 2.73 (s, 3 H), 3.31 (s, 3 H), 3.73 (t, J=5.05 Hz, 2 H), 4.28 (q, J=4.20, 11.82 Hz, 2 H), 4.33 (t, J=5.18 Hz, 2 H)

***N*-(5-(2-Hydroxypropan-2-yl)-3-(2-methoxyethyl)-4-methylthiazol-2(3*H*)-ylidene)-2,2,3,3-tetramethyl-cyclopropanecarboxamide (50)**; A solution of **49** (500 mg, 1.3 mmol, 1 equiv) in 20 mL dry THF was cooled to –78 °C and a 1.6M solution of MeLi in Et_2O (4.25 mL, 6.8 mmol,

5 equiv) was added dropwise. After 30 minutes the reaction was quenched by the addition of 20 mL saturated aqueous NH_4Cl and the solution was extracted with 3x20 mL EtOAc. The combined organic solutions were washed with brine, dried over $MgSO_4$ and subject to column chromatography. The product was obtained in 72% (346 mg, 0.94 mmol) yield as colorless solid; ^{1}H NMR (400 MHz, $CDCl_3$): δ (ppm) = 1.22 (s, 6 H), 1.35 (s, 6 H), 1.55 (s, 1 H), 1.61 (s, 6 H), 2.48 (s, 3 H), 3.33 (s, 3 H), 3.71 (t, *J*=5.43 Hz, 2 H), 4.27 (t, *J*=5.43 Hz, 2 H); ^{13}C NMR (100 MHz, $CDCl_3$): δ (ppm) =12.71, 17.01 (4 C), 24.10 (2 C), 30.37, 31.57 (2 C), 42.34, 45.71, 59.04, 70.07, 100.00, 124.60, 138.45, 182.57; HRMS (ESI+): *m*/*z* (%) = 355.2055, calcd. 355.2055 for $C_{18}H_{31}N_2O_3S^+$ $[M+H]^+$; Elemental analysis: C 60.63, H 8.44, N 7.82, calcd. C 60.98, H 8.53, N 7.90

(*Z*)-*N*-(3-(2-Methoxyethyl)-5-(2-methoxypropan-2-yl)-4-methylthiazol-2(3*H*)-ylidene)-2,2,3,3-tetramethyl-cyclopropanecarboxamide (51), General procedure 2, 79% yield, light yellow solid; ^{1}H NMR (400 MHz, $CDCl_3$): δ (ppm) = 1.22 (s, 6 H), 1.36 (s, 6 H), 1.54 (s, 6 H), 1.56 (s, 1 H), 2.06 (s, 1 H), 2.42 (s, 3 H), 3.05 - 3.19 (m, 3 H), 3.27 - 3.36 (m, 3 H), 3.72 (t, *J*=5.43 Hz, 2 H), 4.28 (t, *J*=5.43 Hz, 2 H); ^{13}C NMR (100MHz, $CDCl_3$): δ (ppm) = 12.02, 17.00 (4 C), 24.10 (2 C), 28.12, 30.43 (2 C), 42.34, 45.71, 50.34, 59.06, 70.01, 120.72, 130.56, 133.96, 181.74

(*Z*)-*N*-(3-(4-Bromobutyl)-4,5-dimethylthiazol-2(3*H*)-ylidene)-2,2,3,3-tetramethyl-cyclopropanecarboxamide (53) 2,2,3,3-Tetramethylcyclopropane acid (1.42 g, 10 mmol, 1 equiv), Et_3N (2.2 mL, 3 mmol, 3 equiv) and BOP (5.7 g, 1.3 mmol, 1.3 equiv) were added to a solution of 4,5-dimethylthiazol-2(3*H*)-imine (**2**, 1.28 g, 10 mmol, 1 equiv) in 15 mL DCM, at 0 °C and the mixture was stirred at room temperature for 20 hours. The reaction was quenched by addition of 20 mL water followed by 50 mL aqueous saturated solution $NaHCO_3$ and 75 mL

EtOAc. The phases were separated and the aqueous phase was washed with 2x50 mL EtOAc. The combined organic fractions were washed with 75 mL brine, dried over $MgSO_4$ and concentrated by rotary evaporation. The obtained residue was purified by column chromatography (silica, EtOAc:Petrolether, 1/9 to 1/4) to give **52** 0.45 g, 18% yield as colorless solid. NaH was added (60% in mineral oil, 33 mg, 0.78 mmol, 2 equiv) to a solution of **52** (100 mg, 0.39 mmol, 1 equiv) in 0.5 mL DMF, and the mixture was stirred for 5 minutes at room temperature after which $Br(CH_2)_4Br$ (0.5 mL, 3.9 mmol, 10 equiv) was added and the whole was stirred overnight at room temperature. The reaction was quenched by addition of H_2O (2 mL), followed by 15 mL aqueous saturated solution $NaHCO_3$ and 20 mL EtOAc, under stirring. The phases were separated, the organic phase was washed with 20 mL EtOAc and the combined organic fractions were dried over $MgSO_4$ and concentrated under reduced pressure. The resulting oil was subjected to column chromatography purification (silica, EtOAc:Petrolether, 1/9 to 1/4) to give 86 mg **53**, 56% yield as colorless solid; ^{1}H NMR (400 MHz, $CDCl_3$): δ (ppm) = 1.23 (s, 6 H), 1.35 (s, 6 H), 1.54 (s, 1 H), 2.02 – 1.79 (m, 4 H), 2.17 (s, 3 H), 2.20 (s, 3 H), 3.53 (t, J=6.0 Hz, 2 H), 4.15 (t, J=6.7 Hz, 2 H); ^{13}C NMR (100 MHz, $CDCl_3$): δ (ppm) = 11.14, 11.64, 17.01 (4 C), 24.09, 27.34, 29.60, 30.13, 33.04, 42.35, 44.96, 113.52, 127.09, 164.52, 181.51; HRMS (ESI+): m/z (%) = 387.1103 calcd. 387.1106 for $C_{17}H_{28}{}^{79}BrN_2OS^+$ $[M+H]^+$

Radioligand Binding Assay

The binding affinity towards CB_1 and CB_2 receptors was determined according to a previously published protocol.[61] In brief, membrane preparations obtained from CHO cell lines stably transfected with either human CB_1 (hCB_1-CHO; obtained from Euroscreen, Gosselies, Belgium) or human CB_2 (hCB_2-CHO; obtained from Paul L. Prather, Department of Pharmacology and

Toxicology, College of Medicine, University of Arkansas for Medical Sciences, USA) were used in combination with [^{3}H]**56** (6,438 GBq/mmol; PerkinElmer Life and Analytical Sciences, Rodgau, Germany) as radioligand. The incubation was performed in binding buffer (50 mM TRIS-HCl, pH 7.4, 0.1% bovine serum albumin (BSA), 5 mM $MgCl_2$, 1 mM EDTA) for 90 min at room temperature. Various concentrations of test compounds were administered and the non-specific binding was determined in the presence of 10 μM **56**. Incubations were terminated by rapid filtration through a GF-B glass fiber filter pre-incubated for 90 min at room temperature in a freshly prepared solution of polyvinylpyrrolidone/Tween 20 (0.5%/0.1%) using a 48-well cell harvester (Brandel, Gaithersburg, MD, USA). Bound radioactivity was analyzed for K_i values using nonlinear regression analysis (GraphPad Prism 2.01), with the K_D values for [^{3}H]**56** determined from saturation experiments.[61]

Radiochemistry

No-carrier-added [^{18}F]fluoride ($t_{1/2}$=109.8 min) was produced via the [^{18}O(p,n)^{18}F] nuclear reaction by irradiation of [^{18}O]H_2O (Hyox 18 enriched water, Rotem Industries Ltd, Israel) on a Cyclone®18/9 (iba RadioPharma Solutions, Belgium) with a fixed energy proton beam using Nirta® [^{18}F]fluoride XL target. All radioactivity measurements were performed with an ISOMED 2010 (MED GmbH, Dresden, Germany) dose calibrator. Radio-TLC plates were further processed using a BAS-1800 II system Bioimaging Analyzer (Fuji Photo Film, Co. Ltd., Tokyo, Japan) and the obtained images were quantified with AIDA 2.31 software (raytest Isotopenmessgeräte GmbH, Straubenhardt, Germany).

For manual optimization, [^{18}F]fluoride was trapped on a Chromafix® 30 PS-HCO_3^- cartridge, eluted with a 20 mg/mL aqueous solution of K_2CO_3 (1.78 mg, 12.9 mmol) and subsequently

added to a 5 mL V vial in the Discover PETwave microwave CEM® (CEM Corporation, Matthews, NC, USA) cavity in the presence of Kryptofix®222 (K2.2.2., 11.2 mg, 29.7 mmol) in 1mL CH_3CN. The aqueous [^{18}F]fluoride was dried under vacuum and argon flow in the microwave cavity (75 W, 20 cycles) at 50-60 °C for 10-12 min. Additional aliquots of CH_3CN (2 x 1.0 mL) were added for azeotropic drying. With regard to the reactive anhydrous K[^{18}F]F-K2.2.2./K_2CO_3 complex, reaction parameters were optimized by varying the amount of the halo precursor **53**, the reaction time, the temperature, the solvent (CH_3CN, DMF, DMSO), and the heating mode (thermal vs. microwave-assisted).

*Automated radiosynthesis of [^{18}F]**29***

Remote-controlled radiosynthesis was performed using a TRACERLab™ FX F-N synthesizer (GE Healthcare, USA) equipped with a PU-980 pump (JASCO, Germany), a WellChrom K-2001 UV detector (KNAUER GmbH, Berlin, Germany), NaI(Tl) counter and automated data acquisition (NINA software version 4.8 rev. 4, Nuclear Interface GmbH, Dortmund, Germany). Reaction conditions were set up as depicted in Figure 3. Briefly, [^{18}F]fluoride (4-10 GBq) was trapped on a Chromafix® 30 PS-HCO_3^- cartridge (entry **1**, MACHEREY-NAGEL GmbH & Co. KG, Düren, Germany) in the remotely controlled synthesis module. [^{18}F]Fluoride was eluted with K_2CO_3 solution (1.78 mg/0.4 mL water; entry **2**) and mixed with K2.2.2 (11.5 mg/1mL CH_3CN; entry **3**)] in the reaction vessel (entry **6**) and azeotropically dried for approximately 10 min. Thereafter, 3.5 mg of the bromo precursor (**53**), dissolved in 1 mL CH_3CN (entry **4**), was added, and the reaction mixture was stirred at 80 °C for 10 min. After cooling, the reaction mixture was diluted with 3 mL H_2O/CH_3CN (1:1, entry **5**) and transferred into the injection vial. Semi-preparative HPLC was performed using the Reprosil-Pur C18-AQ column with a solvent composition of 65% CH_3CN/20 mM aq. NH_4OAc at a flow rate of 4.2 mL/min (entry 7). [^{18}F]**29**

was collected in entry **8** previously loaded with 40 mL H_2O. Final purification was performed by passing the solution through a Sep Pak® C18 light cartridge (entry **11**), followed by washing with 2 mL water (entry **9**) and elution of [^{18}F]**29** with 1.25 mL EtOH (entry **10**) into the product vial (entry **12**). To obtain an injectable solution, the solvent was reduced under a gentle argon stream at 70 °C and the radiotracer was formulated in saline-alcohol solution (90%:10%, NaCl:EtOH).

Radiochemical yield, radiochemical purity and specific activity were assessed following the method described in quality control section.

Quality control

For the radiosynthesis of [^{18}F]**29**, radio-TLC was performed on Polygram® SIL/UV254 plates (Macherey-Nagel, Germany) with petroleum ether/ethyl acetate (PE:EE; 6:4, v/v). The spots of the reference compound were visualized using UV light at 254 nm. Labeling efficiencies and radiochemical purities were determined by radio-TLC and calculated as the percentage of the product peak to the sum of the activity measured. Radio-HPLC was performed on a JASCO LC-2000 system, incorporating a PU-2080*Plus* pump, AS-2055*Plus* auto injector (100 mL sample loop), and a UV-2070*Plus* detector coupled with a gamma radioactivity HPLC detector (Gabi Star, raytest Isotopenmessgeräte GmbH). Labeling efficiencies, radiochemical purities, specific activities and metabolic studies were investigated with analytical radio-HPLC using a Reprosil-Pur C18-AQ (250x4.6 mm, 5 µm) column with an eluent composition of 70 %CH_3CN/20 mM aq. NH_4OAc at a flow rate of 1 mL/min. Data analysis was performed with the Galaxie chromatography software (Agilent Technologies) using the chromatograms obtained at 312 nm.

Determination of in vitro *stability and lipophilicity (Log $D_{7.2}$)*

The *in vitro* radiochemical stability of [^{18}F]**29** was investigated in 0.9% NaCl solution at 40 °C and EtOH at room temperature for up to 90 min. Samples were taken at 15, 30, 60, and 90 min of incubation and analyzed by radio-TLC and radio-HPLC.

The partition coefficient of **29** was calculated theoretically by the commercially available software ACD/Labs. Log $D_{7.4}$ of [^{18}F]**29** was experimentally determined in n-octanol/phosphate-buffered saline (PBS; 0.01 M, pH 7.4) at room temperature by the shake-flask method. The measurement was performed twice in triplicate.

In vitro *Autoradiography*

The *in vitro* autoradiographic experiments were performed according to a previously published protocol[61] using four to six tissue slices (thickness = 12 mikrom) from spleen obtained from two animals. Each tissue slice was delineated as a single ROI (region of interest), the background-corrected intensity per area (in terms of "QL/pixel") for each ROI calculated, and the relative amount of bound activity estimated (incubation with radioligand alone = 100%). In brief, spleen tissue from female SPRD rats (10-12 weeks) was cut into 12 µm thick sections using a cryostat microtome (Microm International GmbH, Walldorf, Germany). The slices were mounted on microscopic glass slides (Superfrost, Menzel, Germany) and stored at –25 °C until use. For autoradiographic experiments, the slides were adapted to room temperature, dried in a stream of cold air, pre-incubated in binding buffer (50 mM TRIS-HCl, pH 7.4, 5% bovine serum albumin (BSA), 5 mM $MgCl_2$, 1 mM EDTA) for 15 min at room temperature and dried again in a stream of cold air. Then, samples were incubated for 1 h at room temperature with [^{18}F]**29** without (total binding) or with **54** (CB_2-selective inverse agonist), **55** (CB_1-selective antagonist), **56** (CB_1/CB_2-selective agonist), or **29**. Thereafter, the samples were washed twice for 2 min at 4 °C in 50 mM TRIS-HCl, pH 7.4, containing 1% BSA, dipped briefly in ice-cold deionized water (5 s), dried in

a stream of cold air, and exposed to appropriate imaging plates (Fuji Photo Film, Co. Ltd., Tokyo, Japan), which were eventually scanned using a HD-CR 35 scanner (raytest Isotopenmessgeraete GmbH, Straubenhardt, Germany). The scan data were visualized and processed by computer-assisted microdensitometry (Aida version 2.31, raytest Isotopenmessgeräte GmbH, Straubenhardt, Germany).

In vivo *metabolism*

[^{18}F]**29** (100 - 150 MBq, 169.7 ± 11.7 GBq/µmol in 150 µL NaCl 0.9%/10% EtOH) was injected *via* the tail vein in CD-1 female mice (10 - 12 weeks old, 20-25 g, n = 3). Blood samples and brain homogenates were obtained at 30 min p.i. Plasma samples were obtained by centrifugation of the blood at 15,000 rpm at 4 °C for 2 min, and the brain tissue was homogenized in ice-cold 50 mM Tris-HCl (pH = 7.4) using a Glass/PTFE Potter Elvehjem tissue grinder (Potter S, B. Braun Biotech International, Sartorius AG, Goettingen, Germany). The samples were vortexed, incubated on ice, and centrifuged at 10,000 rpm for 3 min. Two-fold extractions of plasma and brain samples were performed using ice-cold MeOH/H_2O (9:1, v/v). Supernatants were collected, and the precipitates were re-dissolved in ice-cold MeOH/H_2O (9:1, v/v) for the second extraction. The supernatants from the two extractions were combined, concentrated under a gentle argon stream at 70 °C, analyzed by radio-TLC and gradient analytical HPLC (see section Quality Control). Aliquots from each extraction supernatant and the precipitates were also taken, and quantified by γ counting (Wallac Wizard 1470, Perkin Elmer Inc., Waltham U.S.A.) along with the respective aliquots of intact plasma samples and brain homogenates.

Small-animal PET/MR experiments (Pharmacokinetics and Specificity)

The animals were initially anesthetized with 4% of isoflurane and were positioned prone into a small-animal PET/MR (nanoScan®, MEDISO, Budapest, Hungary) on a heated (37 °C) mouse bed while the respiration rate was continuously monitored. The anesthesia (Anaesthesia Unit U-410, agntho's, Lidingö, Sweden) was maintained at 1.8% isoflurane in a 60% oxygen/40% air gas mixture (Gas blender 100 series, MCQ Instruments, Rome, Italy) with 350 mL/min airflow. Prior to the PET scan a scout image MR sequence was performed to outline the animal dimensions. Female CD-1 mice (n=3, age: 12 weeks, weight: 33.6 ± 2.6 g) received an i.v. injection of 12.0 ± 4.1 MBq [^{18}F]**29**. A dynamic whole body 60 min animal PET scan was started simultaneously and data collected in list mode. Following the PET scan, a T1-weighted whole-body MR scan (gradient echo sequence, TR = 20 ms; TE = 3.2 ms) was performed for anatomical orientation after co-registration and attenuation correction at the reconstruction step (OSEM, 4 iterations, 6 subsets; MR based attenuation correction). After 24 hours of recovery the same animals received an i.p. injection of the specific blocking compound **1** (3 mg/kg) 15 min prior to the i.v. injection of 12.8 ± 5.3 MBq [^{18}F]**29** and simultaneously started PET scan.

Small-animal PET experiments (LPS study)

A small-animal PET/CT scanner ARGUS (Sedecal, Madrid, Spain) was used. In all experiments, a PET session was conducted simultaneously for two mice (LPS-treated and controls, three pairs). CD-1 male mice (25-27 g) were used in all experiments. The LPS-treated mice were injected with LPS (5 mg/kg, ip)[60] 5 days before the PET studies. The experimental animal protocols were approved by the Animal Care and Use Committee of the Johns Hopkins Medical Institutions.

Baseline: One mouse from a pair belonged to the control group whereas the other mouse belonged to the experimental group (LPS-treated). Mice were anesthetized by isoflurane.

Dynamic PET scans were acquired for 30 min (20 s x3, 30 s x2, 1 min x2, 2 min x3, 5 min x4) immediately after an intravenous bolus injection of [^{18}F]**29** (4 - 8 MBq) that was prepared with specific radioactivity of 681 GBq/µmol. A CT scan was acquired shortly before the PET scan and the two images were fused. This was used as a reference for localization of the radiotracer uptake in various brain regions. In all PET experiments, a 250-700 keV energy window was used, and the data were reconstructed using an iterative 2D ordered-subject expectation-maximization method, with a trans-axial pixel size of 0.4 mm and axial slice thickness of 0.8 mm.[62] No attenuation and scatter corrections were applied, as they have a relatively small impact on mouse brain imaging.

*Blocking***:** The LPS-treated mice were injected with the CB_2 selective agonist **1** (3 mg/kg, i.p., 0.1 mL in 50% aqueous DMSO) 15 min before the radiotracer injection, whereas the control mice were injected with 0.1 mL of vehicle solution. The PET experiment was performed similarly to the baseline experiment.

Supporting Information

^{1}H, ^{13}C, COSY 2D, HMBC 2D, NOESY 2D NMRs of compound **44**.

^{1}H NMR of compounds **18**, **19**, **20**, **21**, **23**, **24**, **25**, **26**, **27**, **28**, **29**, **44**, **45**, **50**, **53**.

Molecular formula strings.

AUTHOR INFORMATION

Corresponding Authors

A.G. Horti*: phone, 001 410 614 5130; e-mail, ahorti1@jhmi.edu.

R.-P. Moldovan*: phone, 0049 341 234179 4634; e-mail, r.moldovan@hzdr.de.

Author Contributions

Rodrigo Teodoro, Andrew G. Horti designed and conducted the radiochemical experiments. Rareş-Petru Moldovan, Yongjun Gao and Andrew G. Horti conceived and performed the chemical syntheses. Winnie Deuther-Conrad and Andrew G. Horti planned and performed the radioligand binding studies. Andrew G. Horti, Yuchuan Wang, Hiroto Kuwabara, Masayoshi Nakano, Winnie Deuther-Conrad, Mathias Kranz and Peter Brust designed and performed the PET/MR imaging experiments. Rareş-Petru Moldovan, Rodrigo Teodoro, Yongjun Gao, Winnie Deuther-Conrad, Mathias Kranz, Yuchuan Wang, Hiroto Kuwabara, Masayoshi Nakano, Heather Valentine, Steffen Fischer, M. Pomper, Dean F. Wong, Robert F. Dannals, Peter Brust, Andrew G. Horti analyzed the data, wrote and revised the manuscript.

Funding Sources

This research was supported by NIH grant AG037298 (A.G. Horti), DFG fellowship MO 2677/1-1 (R.-P. Moldovan) and, in part, by Division of Nuclear Medicine of The Johns Hopkins University School of Medicine.

Notes

The authors declare no competing financial interest.

ACKNOWLEDGMENT

We thank Mrs. Tina Spalholz for help with radioligand binding studies Ms. Paige Finley for help with animal experiments and Judy W. Buchanan for editorial help.

ABBREVIATIONS

CB_2, cannabinoid receptors type 2; CB_1, cannabinoid receptors type 1, LPS, lipopolysaccharide; THC, (–)-trans-Δ9-tetrahydrocannabinol; PET, positron emission tomography; DMF, N,N-dimethylformamide; TBAF, tetrabutylammonium fluoride; Et_3N, triethylamine; BOP, (Benzotriazol-1-yloxy)tris(dimethylamino)phosphonium

hexafluorophosphate; K2.2.2., 2.2.2-Cryptand; HPLC, high performance liquid chromatography; SUV, standardized uptake value;

REFERENCES

1. Gaoni, Y.; Mechoulam, R. Isolation, structure, and partial synthesis of an active constituent of Hashish. *J. Am. Chem. Soc.* **1964,** *86*, 1646-1647.

2. Michoulam, R.; Shvo, Y. Hashish. I. The structure of cannabidiol. *Tetrahedron* **1963,** *19*, 2073-2078.

3. McPartland, J. M.; Duncan, M.; Di Marzo, V.; Pertwee, R. G. Are cannabidiol and Δ(9)-tetrahydrocannabivarin negative modulators of the endocannabinoid system? A systematic review. *Br. J. Pharmacol.* **2015,** *172*, 737-753.

4. Svizenska, I.; Dubovy, P.; Sulcova, A. Cannabinoid receptors 1 and 2 (CB_1 and CB_2), their distribution, ligands and functional involvement in nervous system structures-a short review. *Pharmacol. Biochem. Behav.* **2008,** *90*, 501-511.

5. Panagis, G.; Mackey, B.; Vlachou, S. Cannabinoid regulation of brain reward processing with n emphasis on the role of CB_1 receptors: a step back into the future. *Front. Psychiatry* **2014,** *5*, 1-20.

6. Console-Bram, L.; Marcu, J.; Abood, M. E. Cannabinoid receptors: nomenclature and pharmacological principles. *Prog. Neuropsychopharmacol. Biol. Psychiatry* **2012,** *38*, 4-15.

7. Matsuda, L. A.; Lolait, S. J.; Brownstein, M. J.; Young, A. C.; Bonner, T. I. Structure of a cannabinoid receptor and functional expression of the cloned cDNA. *Nature* **1990,** *346*, 561-564.

8. Munro, S.; Thomas, K. L.; Abu-Shaar, M. Molecular characterization of a peripheral receptor for cannabinoids. *Nature* **1993,** *365*, 61-65.

9. Brown, A. J. Novel cannabinoid receptors. *Br. J. Pharmacol.* **2007,** *152*, 567-575.

10. Baker, D.; Pryce, G.; Davies, W. L.; Hiley, C. R. In silico patent searching reveals a new cannabinoid receptor. *Trends Pharmacol. Sci.* **2006,** *27*, 1-4.

11. Overton, H. A.; Babbs, A. J.; Doel, S. M.; Fyfe, M. C.; Gardner, L. S.; Griffin, G.; Jackson, H. C.; Procter, M. J.; Rasamison, C. M.; Tang-Christensen, M.; Widdowson, P. S.; Williams, G. M.; Reynet, C. Deorphanization of a G protein-coupled receptor for oleoylethanolamide and its use in the discovery of small-molecule hypophagic agents. *Cell Metab.* **2006,** *3*, 167-175.

12. Vemuri, V. K.; Makriyannis, A. Medicinal chemistry of cannabinoids. *Clin. Pharmacol. Ther.* **2015,** *97*, 553-558.

13. Roche, M.; Finn, D. P. Brain CB_2 receptors: implications for neuropsychiatric disorders. *Pharmaceuticals* **2010,** *3*, 2517-2553.

14. Horti, A. G.; Van Laere, K. Development of radioligands for *in vivo* imaging of type 1 cannabinoid receptors (CB_1) in human brain. *Curr. Pharm. Des.* **2008,** *14*, 3363-3383.

15. Wong, D. F.; Kuwabara, H.; Horti, A. G.; Raymont, V.; Brasic, J.; Guevara, M.; Ye, W.; Dannals, R. F.; Ravert, H. T.; Nandi, A.; Rahmim, A.; Ming, J. E.; Grachev, I.; Roy, C.; Cascella, N. Quantification of cerebral cannabinoid receptors subtype 1 (CB_1) in healthy subjects and schizophrenia by the novel PET radioligand [^{11}C]OMAR. *NeuroImage* **2010,** *52*, 1505-1513.

16. Onaivi, E. S. Neuropsychobiological evidence for the functional presence and expression of cannabinoid CB_2 receptors in the brain. *Neuropsychobiology* **2006,** *54*, 231-246.

17. Van Sickle, M. D.; Duncan, M.; Kingsley, P. J.; Mouihate, A.; Urbani, P.; Mackie, K.; Stella, N.; Makriyannis, A.; Piomelli, D.; Davison, J. S.; Marnett, L. J.; Di Marzo, V.; Pittman, Q. J.; Patel, K. D.; Sharkey, K. A. Identification and functional characterization of brainstem cannabinoid CB_2 receptors. *Science (New York, N.Y.)* **2005,** *310*, 329-332.

18. Ashton, J. C.; Friberg, D.; Darlington, C. L.; Smith, P. F. Expression of the cannabinoid CB_2 receptor in the rat cerebellum: an immunohistochemical study. *Neurosci. Lett.* **2006,** *396*, 113-116.

19. Sheng, W. S.; Hu, S.; Min, X.; Cabral, G. A.; Lokensgard, J. R.; Peterson, P. K. Synthetic cannabinoid WIN55,212-2 inhibits generation of inflammatory mediators by IL-1beta-stimulated human astrocytes. *Glia* **2005,** *49*, 211-219.

20. Golech, S. A.; McCarron, R. M.; Chen, Y.; Bembry, J.; Lenz, F.; Mechoulam, R.; Shohami, E.; Spatz, M. Human brain endothelium: coexpression and function of vanilloid and endocannabinoid receptors. *Brain Res. Mol. Brain Res.* **2004,** *132*, 87-92.

21. Benito, C.; Nunez, E.; Tolon, R. M.; Carrier, E. J.; Rabano, A.; Hillard, C. J.; Romero, J. Cannabinoid CB_2 receptors and fatty acid amide hydrolase are selectively overexpressed in neuritic plaque-associated glia in Alzheimer's disease brains. *J. Neurosci.* **2003,** *23*, 11136-11141.

22. Benito, C.; Romero, J. P.; Tolon, R. M.; Clemente, D.; Docagne, F.; Hillard, C. J.; Guaza, C.; Romero, J. Cannabinoid CB_1 and CB_2 receptors and fatty acid amide

hydrolase are specific markers of plaque cell subtypes in human multiple sclerosis. *J. Neurosci.* **2007,** *27*, 2396-2402.

23. Yiangou, Y.; Facer, P.; Banati, R. B.; O'Shaughnessy, C. T.; Chessell, I. P.; Anand, P. Cannabinoid receptor CB_2 expression in activated microglia of multiple sclerosis and amyotrophic lateral sclerosis spinal cord. *J. Neurol., Neurosurg. Psychiatry* **2004,** *75*, 1226-1226.

24. Nunez, E.; Benito, C.; Tolon, R. M.; Hillard, C. J.; Griffin, W. S.; Romero, J. Glial expression of cannabinoid CB_2 receptors and fatty acid amide hydrolase are beta amyloid-linked events in Down's syndrome. *Neuroscience* **2008,** *151*, 104-110.

25. Palazuelos, J.; Aguado, T.; Pazos, M. R.; Julien, B.; Carrasco, C.; Resel, E.; Sagredo, O.; Benito, C.; Romero, J.; Azcoitia, I.; Fernandez-Ruiz, J.; Guzman, M.; Galve-Roperh, I. Microglial CB_2 cannabinoid receptors are neuroprotective in Huntington's disease excitotoxicity. *Brain* **2009,** *132*, 3152-3164.

26. Donat, C. K.; Fischer, F.; Walter, B.; Deuther-Conrad, W.; Brodhun, M.; Bauer, R.; Brust, P. Early increase of cannabinoid receptor density after experimental traumatic brain injury in the newborn piglet. *Acta Neurobiol. Exp.* **2014,** *74*, 197-210.

27. Páldyová, E.; Bereczki, E.; Sántha, M.; Wenger, T.; Borsodi, A.; Benyhe, S. Noladin ether, a putative endocannabinoid, inhibits μ-opioid receptor activation *via* CB_2 cannabinoid receptors. *Neurochem. Int.* **2008,** *52*, 321-328.

28. Benito, C.; Kim, W. K.; Chavarria, I.; Hillard, C. J.; Mackie, K.; Tolon, R. M.; Williams, K.; Romero, J. A glial endogenous cannabinoid system is upregulated in the brains of macaques with simian immunodeficiency virus-induced encephalitis. *J. Neurosci.* **2005,** *25*, 2530-2536.

29. Chakravarti, B.; Ravi, J.; Ganju, R. K. Cannabinoids as therapeutic agents in cancer: current status and future implications. *Oncotarget* **2014,** *5*, 5852-5872.

30. Ellert-Miklaszewska, A.; Ciechomska, I.; Kaminska, B. Cannabinoid signaling in glioma cells. *Adv. Exp. Med. Biol.* **2013,** *986*, 209-220.

31. Evens, N.; Bormans, G. M. Non-invasive imaging of the type 2 cannabinoid receptor, focus on positron emission tomography. *Curr. Top. Med. Chem.* **2010,** *10*, 1527-1543.

32. Ory, D.; Celen, S.; Verbruggen, A.; Bormans, G. PET radioligands for *in vivo* visualization of neuroinflammation. *Curr. Pharm. Des.* **2014,** *20*, 5897-5913.

33. Yang, P.; Wang, L.; Xie, X. Q. Latest advances in novel cannabinoid CB_2 ligands for drug abuse and their therapeutic potential. *Future Med. Chem.* **2012,** *4*, 187-204.

34. Kohnz, R. A.; Nomura, D. K. Chemical approaches to therapeutically target the metabolism and signaling of the endocannabinoid 2-AG and eicosanoids. *Chem. Soc. Rev.* **2014,** *43*, 6859-6869.

35. Han, S.; Thatte, J.; Buzard, D. J.; Jones, R. M. Therapeutic utility of cannabinoid receptor type 2 (CB_2) selective agonists. *J. Med. Chem.* **2013,** *56*, 8224-8256.

36. Aso, E.; Ferrer, I. Cannabinoids for treatment of Alzheimer's disease: moving toward the clinic. *Front. Pharmacol.* **2014,** *5*, 37.

37. Varley, J.; Brooks, D. J.; Edison, P. Imaging neuroinflammation in Alzheimer's and other dementias: Recent advances and future directions. *Alzheimer's Dementia* **2014**, 1-11.

38. Dhopeshwarkar, A.; Mackie, K. CB_2 Cannabinoid receptors as a therapeutic target-what does the future hold?. *Mol. Pharmacol.* **2014,** *86*, 430-437.

39. Slavik, R.; Bieri, D.; Cermak, S.; Muller, A.; Kramer, S. D.; Weber, M.; Schibli, R.; Ametamey, S. M.; Mu, L. Development and evaluation of novel PET tracers for imaging cannabinoid receptor type 2 in brain. *Chimia* **2014,** *68*, 208-210.

40. Horti, A. G., Raymont, V., Terry, G. E. PET imaging of endocannabinoid system. In *PET and SPECT of Neurobiological Systems*, Dierckx, R. A. J. O., Otte, A., de Vries, E.F.J., van Waarde, A., Luiten, P.G.M. , Ed. Springer: Springer, New York, 2014; pp 249-319.

41. Casteels, C.; Ahmad, R.; Vandenbulcke, M.; Vandenberghe, W.; Van Laere, K. Chapter 4 - Cannabinoids and Huntington's disease. In *Cannabinoids in Neurologic and Mental Disease*, Academic Press: San Diego, 2015; pp 61-97.

42. Horti, A. G.; Gao, Y.; Ravert, H. T.; Finley, P.; Valentine, H.; Wong, D. F.; Endres, C. J.; Savonenko, A. V.; Dannals, R. F. Synthesis and biodistribution of [^{11}C]A-836339, a new potential radioligand for PET imaging of cannabinoid type 2 receptors (CB_2). *Bioorg. Med. Chem.* **2010,** *18*, 5202-5207.

43. Savonenko, A. V.; Melnikova, T.; Wang, Y.; Ravert, H.; Gao, Y.; Koppel, J.; Lee, D.; Pletnikova, O.; Cho, E.; Sayyida, N.; Hiatt, A.; Troncoso, J.; Davies, P.; Dannals, R. F.; Pomper, M. G.; Horti, A. G. Cannabinoid CB_2 receptors in a mouse model of Aβ amyloidosis: immunohistochemical analysis and suitability as a PET biomarker of neuroinflammation. *PLoS One* **2015,** *10*, e0129618.

44. Evens, N.; Vandeputte, C.; Coolen, C.; Janssen, P.; Sciot, R.; Baekelandt, V.; Verbruggen, A. M.; Debyser, Z.; Van Laere, K.; Bormans, G. M. Preclinical evaluation of [^{11}C]NE40, a type 2 cannabinoid receptor PET tracer. *Nucl. Med. Biol.* **2012,** *39*, 389-399.

45. Ahmad, R.; Koole, M.; Evens, N.; Serdons, K.; Verbruggen, A.; Bormans, G.; Van Laere, K. Whole-body biodistribution and radiation dosimetry of the cannabinoid type 2 receptor ligand [^{11}C]NE40 in healthy subjects. *Mol. Imaging Biol.* **2013,** *15*, 384-390.

46. Postnov, A.; Ahmad, R.; Evens, N.; Versijpt, J.; Vandenbulcke, M.; Yaqub, M.; Verbruggen, A.; Bormans, G.; Vandenberghe, W.; Van Laere, K. Quantification of [^{11}C]NE40, a novel PET radioligand for CB_2 receptor imaging. *J. Nucl. Med.* **2013,** *54*, 188.

47. Hortala, L.; Arnaud, J.; Roux, P.; Oustric, D.; Boulu, L.; Oury-Donat, F.; Avenet, P.; Rooney, T.; Alagille, D.; Barret, O.; Tamagnan, G.; Barth, F. Synthesis and preliminary evaluation of a new fluorine-18 labelled triazine derivative for PET imaging of cannabinoid CB_2 receptor. *Bioorg. Med. Chem. Lett.* **2014,** *24*, 283-287.

48. Yrjölä, S.; Sarparanta, M.; Airaksinen, A. J.; Hytti, M.; Kauppinen, A.; Pasonen-Seppanen, S.; Adinolfi, B.; Nieri, P.; Manera, C.; Keinanen, O.; Poso, A.; Nevalainen, T. J.; Parkkari, T. Synthesis, *in vitro* and *in vivo* evaluation of 1,3,5-triazines as cannabinoid CB_2 receptor agonists. *Eur. J. Pharm. Sci.* **2015,** *67*, 85-96.

49. Slavik, R.; Herde, A. M.; Bieri, D.; Weber, M.; Schibli, R.; Kramer, S. D.; Ametamey, S. M.; Mu, L. Synthesis, radiolabeling and evaluation of novel 4-oxo-quinoline derivatives as PET tracers for imaging cannabinoid type 2 receptor. *Eur. J. Med. Chem.* **2015,** *92c*, 554-564.

50. Slavik, R.; Grether, U.; Müller Herde, A.; Gobbi, L.; Fingerle, J.; Ullmer, C.; Krämer, S. D.; Schibli, R.; Mu, L.; Ametamey, S. M. Discovery of a high affinity and selective pyridine analog as a potential positron emission tomography imaging agent for cannabinoid type 2 receptor. *J. Med. Chem.* **2015,** *58*, 4266-4277.

51. Dart, M. J.; Carroll, W. A.; Florjancic, A. S.; Frost, J. M.; Gallagher, M. E.; Li, T.; Nelson, D. W.; Patel, M. V.; Peddi, S.; Perez-Medrano, A. Thiazole compounds as cannabinoid receptor ligands and uses thereof. In WO2007140385 A2: 2007.

52. Yao, B. B.; Hsieh, G.; Daza, A. V.; Fan, Y.; Grayson, G. K.; Garrison, T. R.; El Kouhen, O.; Hooker, B. A.; Pai, M.; Wensink, E. J.; Salyers, A. K.; Chandran, P.; Zhu, C. Z.; Zhong, C.; Ryther, K.; Gallagher, M. E.; Chin, C. L.; Tovcimak, A. E.; Hradil, V. P.; Fox, G. B.; Dart, M. J.; Honore, P.; Meyer, M. D. Characterization of a cannabinoid CB_2 receptor-selective agonist, A-836339 [2,2,3,3-tetramethyl-cyclopropanecarboxylic acid [3-(2-methoxy-ethyl)-4,5-dimethyl-3H-thiazol-(2*Z*)-ylidene]-amide], using *in vitro* pharmacological assays, *in vivo* pain models, and pharmacological magnetic resonance imaging. *J. Pharmacol. Exp. Ther.* **2009,** *328*, 141-151.

53. Friscourt, F.; Fahrni, C. J.; Boons, G.-J. A fluorogenic probe for the catalyst-free detection of azide-tagged molecules. *J. Am. Chem. Soc.* **2012,** *134*, 18809-18815.

54. Cui, M.; Wang, X.; Yu, P.; Zhang, J.; Li, Z.; Zhang, X.; Yang, Y.; Ono, M.; Jia, H.; Saji, H.; Liu, B. Synthesis and evaluation of novel ^{18}F labeled 2-pyridinylbenzoxazole and 2-pyridinylbenzothiazole derivatives as ligands for positron emission tomography (PET) imaging of *β*-amyloid plaques. *J. Med. Chem.* **2012,** *55*, 9283-9296.

55. Bonner, T. G.; Lewis, D.; Rutter, K. Opening of cyclic acetals by trichloro-, dichloro-, and tribromo-borane. *J. Chem. Soc., Perkin Trans. 1.* **1981**, 1807-1810.

56. Albrecht, S.; Defoin, A.; Tarnus, C. Simple preparation of *O*-substituted hydroxylamines from alcohols. *Synthesis* **2006,** 1635-1638.

57. Milewska, M. J.; Gdaniec, M.; Poloński, T. Synthesis, stereochemistry, and chiroptical spectra of cyclopropyl lactones and thionolactones. *Tetrahedron: Asymmetry* **1996,** *7*, 3169-3180.

58. Kirihara, M.; Ogawa, S.; Noguchi, T.; Okubo, K.; Monma, Y.; Shimizu, I.; Shimosaki, R.; Hatano, A.; Hirai, Y. Chemoselective bromination of active methylene and methyne compounds by potassium bromide, hydrochloric acid and hydrogen peroxide. *Synlett* **2006,** *2006*, 2287-2289.

59. Lynn, A. B.; Herkenham, M. Localization of cannabinoid receptors and nonsaturable high-density cannabinoid binding sites in peripheral tissues of the rat: implications for receptor-mediated immune modulation by cannabinoids. *J. Pharmacol. Exp. Ther.* **1994,** *268*, 1612-1623.

60. Qin, L.; Wu, X.; Block, M. L.; Liu, Y.; Breese, G. R.; Hong, J.-S.; Knapp, D. J.; Crews, F. T. Systemic LPS causes chronic neuroinflammation and progressive neurodegeneration. *Glia* **2007,** *55*, 453-462.

61. Rühl, T.; Deuther-Conrad, W.; Fischer, S.; Günther, R.; Hennig, L.; Krautscheid, H.; Brust, P. Cannabinoid receptor type 2 (CB_2)-selective *N*-aryl-oxadiazolyl-propionamides: synthesis, radiolabelling, molecular modelling and biological evaluation. *Org. Med. Chem. Lett.* **2012,** *2*, 32-32.

62. Wang, Y.; Seidel, J.; Tsui, B. M. W.; Vaquero, J. J.; Pomper, M. G. Performance evaluation of the GE healthcare eXplore VISTA dual-ring small-animal PET scanner. *J. Nucl. Med.* **2006,** *47*, 1891-1900.

Table of Contents Graphic

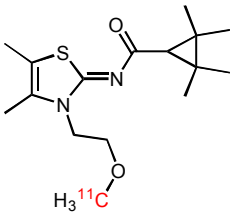

$K_i(CB_2)$ = 0.7 nM
$K_i(CB_1)$ = 270 nM

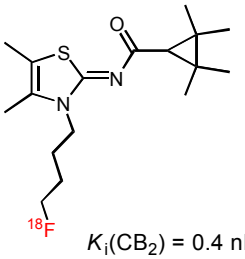

$K_i(CB_2)$ = 0.4 nM
$K_i(CB_1)$ = 380 nM